ACS Chemical Neuroscience

pubs.acs.org/chemneuro

Research Article

Three-Dimensional Tracking of Intracellular Calcium and Redox State during Real-Time Control in a Hypoxic Gradient in Microglia Culture: Comparison of the Channel Blocker and Reoxygenation under Ischemic Shock

Vaibhav Dhyani, Saurabh Kumar, Shanmukh Reddy Manne, Inderjeet Kaur, Soumya Jana, Sarah Russell, Rahuldeb Sarkar, and Lopamudra Giri*

Cite This: *ACS Chem. Neurosci.* 2023, 14, 1810–1825

Read Online

ACCESS | Metrics & More | Article Recommendations | Supporting Information

ABSTRACT: Real-time three-dimensional (3-D) imaging is crucial for quantifying correlations among various molecules under acute ischemic stroke. Insights into such correlations may be decisive in selecting molecules capable of providing a protective effect within a shorter period. The major bottleneck is maintaining the cultures under severely hypoxic conditions while simultaneously 3-D imaging intracellular organelles with a microscope. Moreover, comparing the protective effect of drugs and reoxygenation remains challenging. To address this, we propose a novel workflow for the induction of gas-environment-based hypoxia in the HMC-3 cells along with 3-D imaging using laser-scanning-confocal microscopy. The imaging framework is complemented with a pipeline for quantifying time-lapse videos and cell-state classification. First, we show an imaging-based assessment of the in vitro model for hypoxia using a steep gradient in O_2 with time. Second, we demonstrate the correlation between mitochondrial superoxide production and cytosolic calcium under acute hypoxia. We then test the efficacy of an L-type calcium channel blocker, compare the results with reoxygenation, and show that the blocker alleviates hypoxic conditions in terms of cytosolic calcium and viability within an acute window of one hour. Furthermore, we show that the drug reduces the expression of oxidative stress markers (*HIF1A* and *OXR1*) within the same time window. In the future, this model can also be used to investigate drug toxicity and efficacy under ischemic conditions.

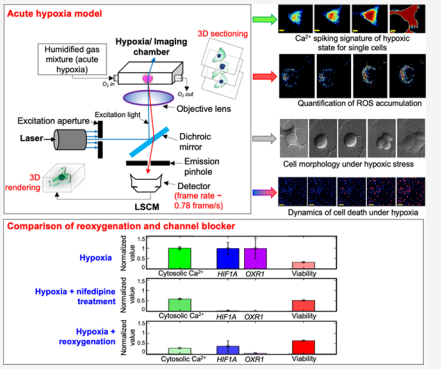

KEYWORDS: *hypoxia, microglia, HMC-3, calcium, Hoechst 33342, Fluo-4AM, Rhod-2AM, MitoSOX Red, HIF1A, OXR1*

1. INTRODUCTION

The central nervous system is most vulnerable to oxidative stresses caused by conditions such as stroke.[1,2] Microglia are the primary macrophages in the brain that undergo activation under hypoxic stress and cause neuroinflammatory responses.[2−4] These cells are the first responders to the changes in the brain microenvironment and activate downstream cell signaling at the early onset of stroke.[5] The toxic neuroinflammatory agents produced by activated microglia under hypoxic conditions aggravate neuronal injury during cerebral ischemia.[6] Increasing evidence indicates that hypoxia-induced upregulation of hypoxia-inducible factor-1α (*HIF1A*) results in apoptotic and autophagic cell death of microglia.[7,8] Thus, microglia provide a feasible target for early intervention for neuroprotection.[9,10]

To design interventions for ischemic stroke, it is essential to understand the abrupt changes in microglia signaling when subjected to ischemic injury.[5,11] In particular, an in vitro model for ischemic shock may allow a better understanding of the time scale of cell morphology changes, cell migration, and calcium (Ca^{2+}) dynamics during microglia activation.[1,12] Such a model may also help identify therapeutic drugs for treating stroke patients in the early phase following ischemia onset to reduce the microglial activation until definitive revascularization therapies can be instituted. Although there are several advanced hypoxia models based on microfluidic structures[13] and cells encapsulated in hydrogels[14,15] that mimic the physiological stress mimicking cancer conditions, they are not relevant for instantaneous live imaging under acute stroke-like conditions.

Apart from stroke-specific models, other disease models, including neurodegeneration,[16] chronic obstructive pulmonary

Received: December 27, 2022
Accepted: April 11, 2023
Published: May 9, 2023

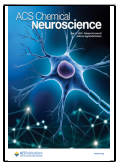

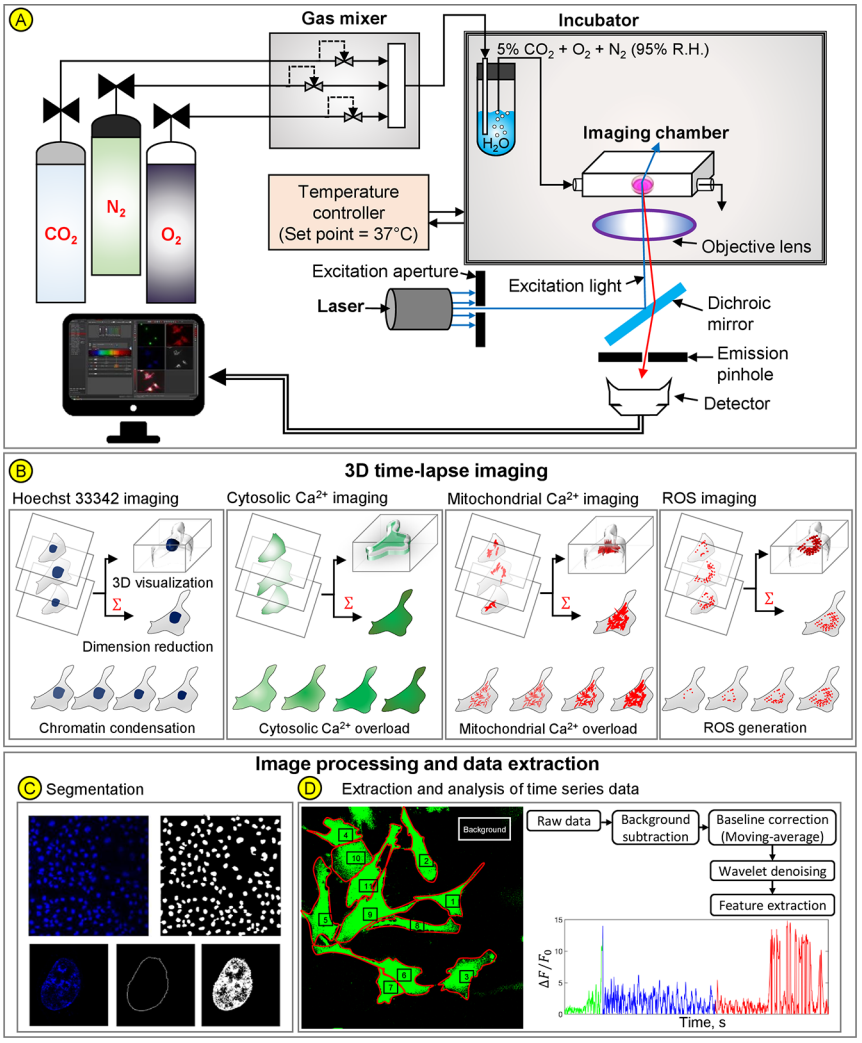

Figure 1. Schematic representation of the setup used for imaging HMC-3 cells under hypoxic stress and analysis of imaging data. (A) Confocal assembly attached to the hypoxia incubator for in situ imaging of cells under hypoxic stress. (B) 3-D time-lapse video acquisition for chromatin condensation, cytosolic Ca^{2+}, mitochondrial Ca^{2+}, and ROS. (C) Application of image segmentation for cell counting and estimation of nucleus cross-sectional area. (D) Workflow for data extraction from time-lapse videos.

disease,[17] and tumor microenvironment,[18] heavily depend on the $CoCl_2$-based hypoxia model because it allows the experimentalist to open the culture plate many times while maintaining the stabilization of HIF. In our previous work, we attempted to create a $CoCl_2$-based hypoxia model for understanding the hypoxic markers for lung epithelial cells in the context of COVID-19.[19] However, such an approach neither allows the implementation of acute ischemic shock nor permits reoxygenation without media reperfusion. Therefore, a gas chamber-based hypoxia model is better suited for creating acute ischemic shock.[20]

Although there are neuronal cell culture[21] and hippocampal slice culture[22] based systems that mimic chronic as well as acute hypoxia and evaluate the redox state, there is limited work on mimicking acute stress in microglia that focuses on imaging the mitochondrial Ca^{2+} and redox status. On the other hand, there are several studies on microglial activation under ischemic stress in vivo.[7,8,23,24] There are fewer cell-line-based studies on the ischemic model for microglia and investigation of molecular markers.[20,25−27] Numerous studies have used a standalone incubator with the O_2 control system to monitor the effects of hypoxic stress on cell proliferation or hypoxia markers in cell cultures (Supplementary Table S1). A standalone incubator-based hypoxia model was used in the study of Voelz et al.[20] to examine the effect of <0.1% O_2 environment on the expression of microRNA regulating proteins in the HMC-3 cell line. In another chamber-based model by Butturini et al.,[25] M1 microglia activation under acute hypoxic stress and its correlation to STAT1 activation is shown in the BV2 cell culture model. Although such a chamber setup can be used to create ischemic stress using severe hypoxia, it has the inherent disadvantage of being unable to perform real-time monitoring of molecular features and correlating to the gene expression patterns. This is because the sample returns to normoxia as soon as it is taken out of the chamber for imaging. Hence, it is difficult to identify the dynamic patterns of various secondary messengers that regulate microglial activation, gene expression levels, and subsequent cell fate under acute hypoxia. Another disadvantage of using the chamber-based hypoxia is that it is difficult to have real-time control of O_2 as the chamber size is rather large.[28]

In this context, a gas environment-based hypoxia chamber with a reduced size that permits real-time control of acute hypoxia and is attached to a high-resolution microscope would

https://doi.org/10.1021/acschemneuro.2c00807
ACS Chem. Neurosci. 2023, 14, 1810−1825

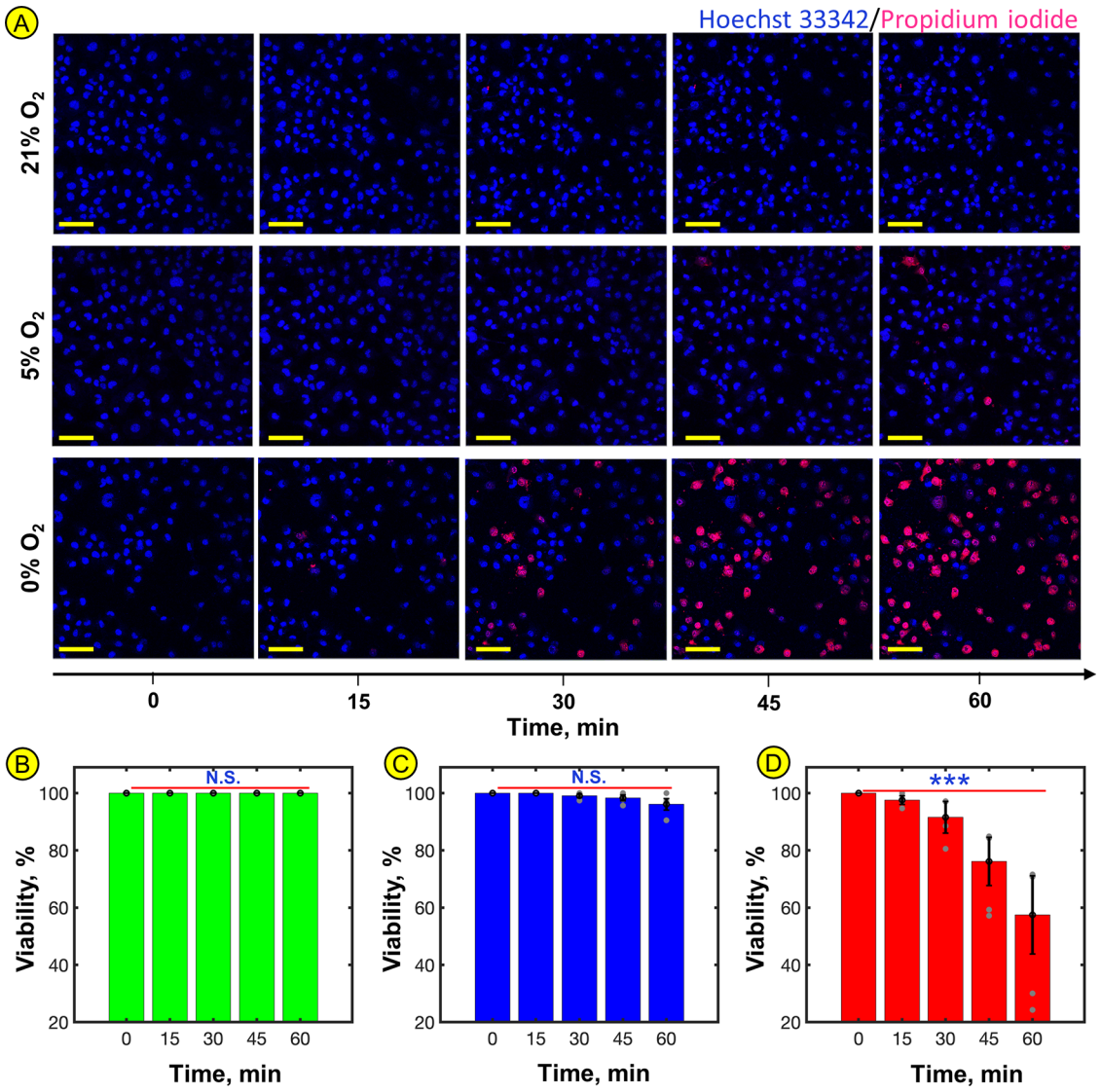

Figure 2. Quantification of viability for hour-long imaging at different O_2 environments inside the incubator attached to the confocal microscope. (A) Microscopy images for representative populations of Hoechst 33342/propidium iodide (PI)-stained HMC-3 cells at 21 (control), 5, and 0% O_2 environments, respectively. Each image is a merge of different z-stacks so that out-of-focus cells can also be accounted for. Blue (Hoechst 33342 stain) indicates nuclei of all cells, live or dead. Red (PI stain) indicates the dead cells (scale bar = 100 μm). (B–D) Bar charts presenting the viability profile for 21 (control), 5, and 0% O_2 environments obtained by quantifying Hoechst 33342/PI double stain time-lapse videos. The graphs indicate each case's mean and S.E.M. from three independent time-lapse videos. A statistically significant decrease in cell viability within one hour of treatment was observed only in the case of a 0% O_2 environment ($p < 0.05$(*), $p < 0.01$(**), $p < 0.001$(***), and $p > 0.5$ (N.S.—no significance), one-way Kruskal Wallis test).

be a step forward for assessing drugs. This paper demonstrates a novel approach for live-cell imaging of cellular responses in microglia cells under ischemic conditions. Our approach is based on adapting a laser-scanning-confocal microscopy (LSCM) system by mounting a hypoxia chamber on top of the confocal objective, which allows the induction of a steep O_2 gradient and provides a means to perform three-dimensional (3-D) imaging and obtain dynamic information from single cells. While microscope-compatible stage-top configurations of hypoxia chambers have been demonstrated in refs 29–32, to the best of our knowledge, no work reports dynamic monitoring of microglia cells under real-time control of hypoxia. Since the changes in Ca^{2+} transients in microglia may represent a disease signature,[33−35] we specifically performed LSCM imaging of cytosolic and mitochondrial Ca^{2+} and superoxide generation in the microglia line while maintaining a hypoxic gradient with respect to time. The recent models with a stage-top configuration mainly focus on ATP metabolism and redox state in cardiomyocytes[31] and AML12 liver cells.[32] In contrast, the current model explores the dynamics of mitochondrial and cytosolic Ca^{2+} in the context of acute stress in microglia. We have also developed a pipeline for semiautomated image analysis and processing of time-series data generated by 3-D live-cell imaging experiments.

The first objective of this study is to calibrate the hypoxia model in terms of dynamic changes in cell morphology, cell viability, migratory behavior, and dissolved O_2 (DO) of the culture media upon treatment with different O_2 levels. Next, we design a steep gradient of hypoxia to simulate the ischemic condition and observe various second messengers as the cellular marker of hypoxia. In the second objective, we identify

https://doi.org/10.1021/acschemneuro.2c00807
ACS Chem. Neurosci. 2023, 14, 1810−1825

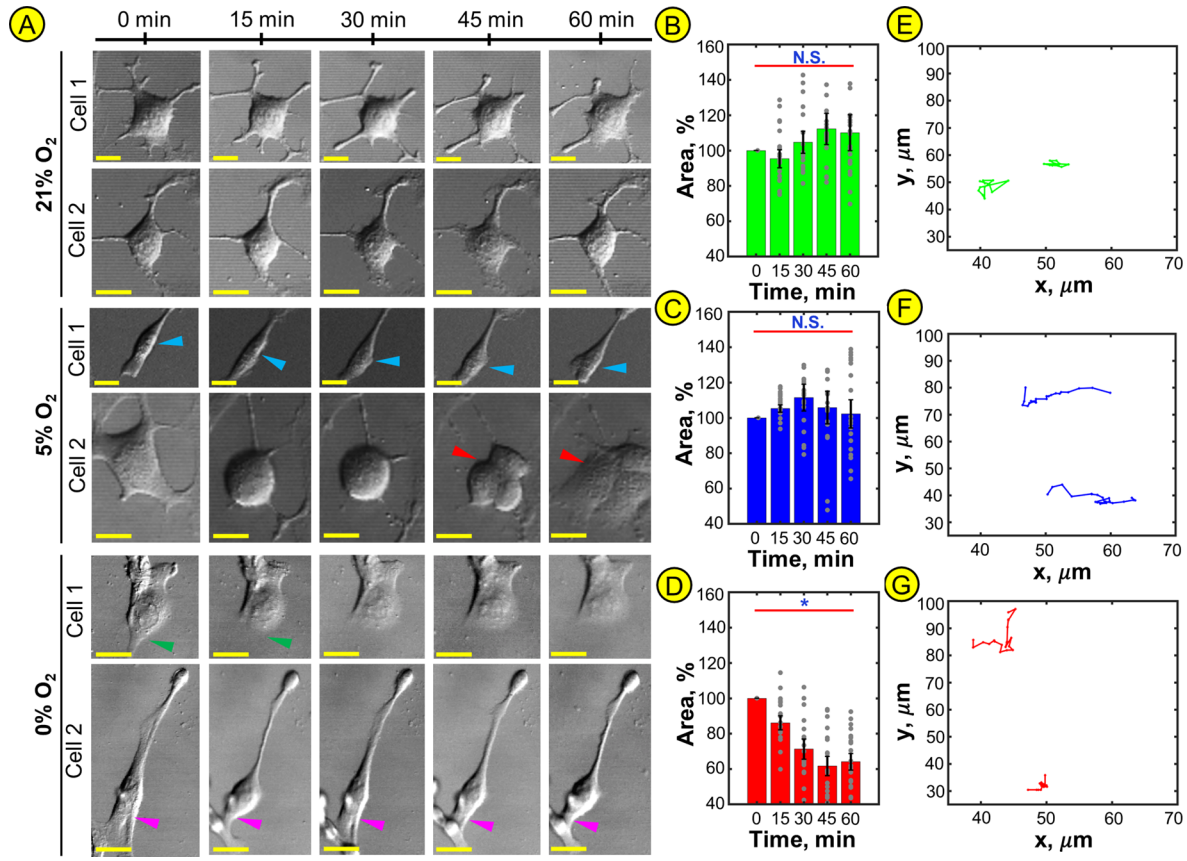

Figure 3. Quantification of changes in the HMC-3 cell shape and cell migration for hour-long imaging at different O_2 environments inside the incubator attached to a confocal microscope: (A) Effects of control (21% O_2) and acute (1 h) hypoxia (5 and 0% O_2) on microglia morphology of the HMC-3 cells. Microglia migration and cell proliferation are observed in the 5% O_2 environment, whereas characteristic signs of cell death, like cellular shrinkage and blebbing of cell membranes, are observed in 0% O_2 environments. (B−D) Bar charts representing shrinkage of cell bodies (cell area) under 21, 5, and 0% O_2 environments, respectively. Statistically significant shrinkage of cell area within 1 hour of treatment was observed only in the case of a 0% O_2 environment ($p < 0.05$(*), $p < 0.01$(**), $p < 0.001$(***), and $p > 0.5$ (N.S.—no significance), one-way Kruskal Wallis test). (E−G) Traces of cell centroids for representative cells under 21, 5, and 0% O_2 environments, respectively. For each O_2 environment, two representative cells are shown.

the time window for the onset of Ca^{2+} entry in the cytosol and the overloading of mitochondrial Ca^{2+}. We also establish the correlation of cytosolic and mitochondrial Ca^{2+} with mitochondrial superoxide production. Since cytosolic Ca^{2+} was found to be the early marker, we chose to test a Ca^{2+} channel blocker (CCB) to protect the cells under ischemic conditions within a short period. Third, we demonstrate that the proposed platform can be used to compare channel blocker's efficacy with reoxygenation. In this study, we performed RT-PCR experiments to identify the link between the overloading of Ca^{2+} and the increase in oxidative stress markers (*HIF1A*, *OXR1*) within an acute window of 1 hour. We specifically chose nifedipine in the third objective, as it is an L-type CCB, and its antineuroinflammatory effect on microglia cells has been prophylactically reported.[23,36] Using this setup, we show that nonprophylactic CCBs can be a potential approach for modification of cell state within a short period of acute hypoxia when immediate reoxygenation is not possible. To the best of our knowledge, a setup with the chamber attached to the microscope has not been implemented earlier to study the consequences of ischemic conditions on microglia through imaging in combination with gene expression studies.

2. RESULTS

2.1. Calibration of the Hypoxia Setup. *2.1.1. Hypoxic Stress Leads to Morphological Changes and Decreases the Viability of the HMC-3 Cells.* In most ischemic shock experiments, the median O_2 levels fall to 2−0%.[20,37] PbO_2 values <10 mm Hg are linked with a higher risk for ischemic brain injury.[38] In order to determine the dynamic signatures of biomolecules and morphologies under various hypoxic conditions in HMC-3 cell culture, we studied two levels of hypoxia, 5 and 0% O_2, in the incubation chamber attached to LSCM (Figure 1A). On the other hand, the control condition was studied using 21% O_2. We performed imaging over 60 min to obtain the viability profile in real time. The results show that the control cells with 21% O_2 show no significant change in viability. It can be observed from Figure 2A and Supplementary Video S1 that compared to the control (Figure 2B), the cells subjected to 5% O_2 retained up to 96.10 ± 1.99 (S.E.M.)% viability after 1 h of imaging (Figure 2C). In contrast, the viability in the cell populations subjected to 0% O_2 dropped to 49 ± 10.97 (S.E.M.)% within the same duration of 1 h (Figure 2D). A significant condensation of chromatin over 1 hour was also observed in the case of 5 and 0% O_2 environments (Supplementary Figure S1). The results show that 0% O_2 hypoxia in the incubation chamber attached to

https://doi.org/10.1021/acschemneuro.2c00807
ACS Chem. Neurosci. 2023, 14, 1810−1825

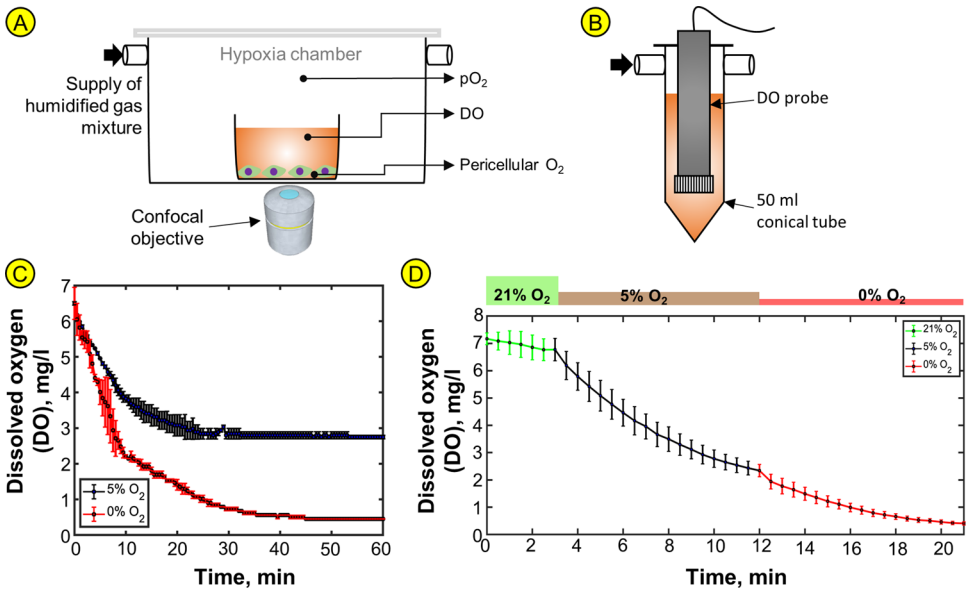

Figure 4. Measurement of the DO gradient in the culture media. (A) Schematic drawing showing the partial pressure (pO_2), DO and pericellular O_2 in the Petri dish kept in the hypoxia chamber. (B) Measurement of DO using a hand-held DO meter in the culture media. (C) Levels of DO as a function of time in the cell culture media when gas mixtures of 5% CO_2 with 5 or 0% O_2 are passed over the culture media at a flow rate of 40 L/h for 1 h. (D) DO gradient created in culture media obtained by providing 21% (3 min), 5% (9 min), and 0% O_2 (9 min) to the hypoxia chamber sequentially.

LSCM can be further investigated to visualize the dynamics of the cell physiology under ischemic shock.[20,39]

One of the major clinical features of hypoxic conditions is the change in the cell shape, and it can therefore be useful to calibrate the shape change as a function of hypoxic stress level. To quantify the correlation between the cell size and hypoxia level, we measured the cross-sectional cell area as a function of the O_2 level. The differential interference contrast (DIC) images depicting the cell morphologies of representative cells at 21, 5, and 0% O_2 levels are shown in Figure 3A. Figure 3B,C shows that at 21 and 5% O_2 environments, no significant change in the cell area occurs in the time window of 1 hour. However, a significant decrease ($p < 0.01$) in the cellular area is observed when subjected to a 0% O_2 environment (Figure 3D). The results show a 38.70 ± 5.92% decrease in the cell area under hypoxic stress at 0% O_2. The DIC time-lapse of the whole population is shown in Supplementary Figure S2 and Supplementary Video S2. In the case of 5% O_2 some cells undergo proliferation (Supplementary Figure S3), which could be attributed to the survival mechanism at that condition. Compared to the 21% O_2 environment, active migration was observed in the case of 5% O_2 environments. Upon quantification of cell centroid migration, it was observed that the centroids of the cells imaged under 21% O_2 migrate at an average speed of 23.40 ± 4.72 (S.E.M.) μm/h (Figure 3E and Supplementary Video S3). In contrast, the average speeds of the cells imaged under 5% (Figure 3F and Supplementary Video S4) and 0% O_2 (Figure 3G and Supplementary Video S5) environments were 69.33 ± 1.90 (S.E.M.) μm/h and 31.75 ± 18.21 (S.E.M.) μm/h respectively. The data reveal that, within a window of 1 h, 5% O_2 induces a significant increase in the migration level and tries to recover the hypoxic injury. In contrast, the 0% O_2 provides a significant shock to induce cell death and reduced migration levels (Supplementary Figure S4). The results show that time-lapse imaging of cell shape using LSCM imaging can measure the displacement of cells as a function of time under hypoxic conditions. In contrast to scratch assay, this can be potentially used to measure cell shape and velocity in real time.

2.1.2. Dynamic Monitoring of DO in Cell Culture Media under Hypoxic Conditions. Although the partial pressure of O_2 in the hypoxia chamber correlates with the pericellular O_2 levels (Figure 4A), it is more accurate to present the DO level in the culture media as it better reflects the stress induced in the system. To measure the O_2 gradient, we measured the real-time values of DO levels in culture media upon hypoxia treatment (Figure 4B). The results show that the O_2 levels decrease with time and reach 2.70 mg/L (~60.46 mmHg) and 0.40 mg/L (~8.95 mmHg) within 1 hour for 5 and 0% O_2 environments, respectively (Figure 4C). These findings demonstrate that the proposed method is able to establish a gradient input in culture by setting a fixed percentage of O_2 in the incubation chamber. Based on this result, we assess cell death dynamics and migration characteristics under a 0% environment, taken as the ischemic shock model. From Figure 4C, it can be concluded that 0% O_2 is suitable to attain 0.6−0.7 mg/L within 30−35 min which is in the range of O_2 levels investigated in several diseases.[14,40]

Next, we focus on investigating the correlation among various molecules that are crucial and can be targeted for designing therapeutics during sudden hypoxic shock. Since cell death was not observed in the first 8−10 min of hypoxia treatment, for each hypoxia level, a nine-minute window was specifically chosen for continuous monitoring of preapoptotic or prelytic conditions through imaging of cytosolic Ca^{2+} and mitochondrial Ca^{2+} dynamics in single cells. For this, we designed a hypoxic gradient with time (Figure 4D), where the DO levels dynamically decrease when cells are subjected to a 21% O_2 environment for 3 min (baseline), followed by 9 min in 5%, and then 9 min in 0% O_2 environments sequentially (total duration of experiment = 21 min). No cell death but the onset of nuclear condensation was observed in this study window, allowing the further characterization of preapoptotic

https://doi.org/10.1021/acschemneuro.2c00807
ACS Chem. Neurosci. 2023, 14, 1810−1825

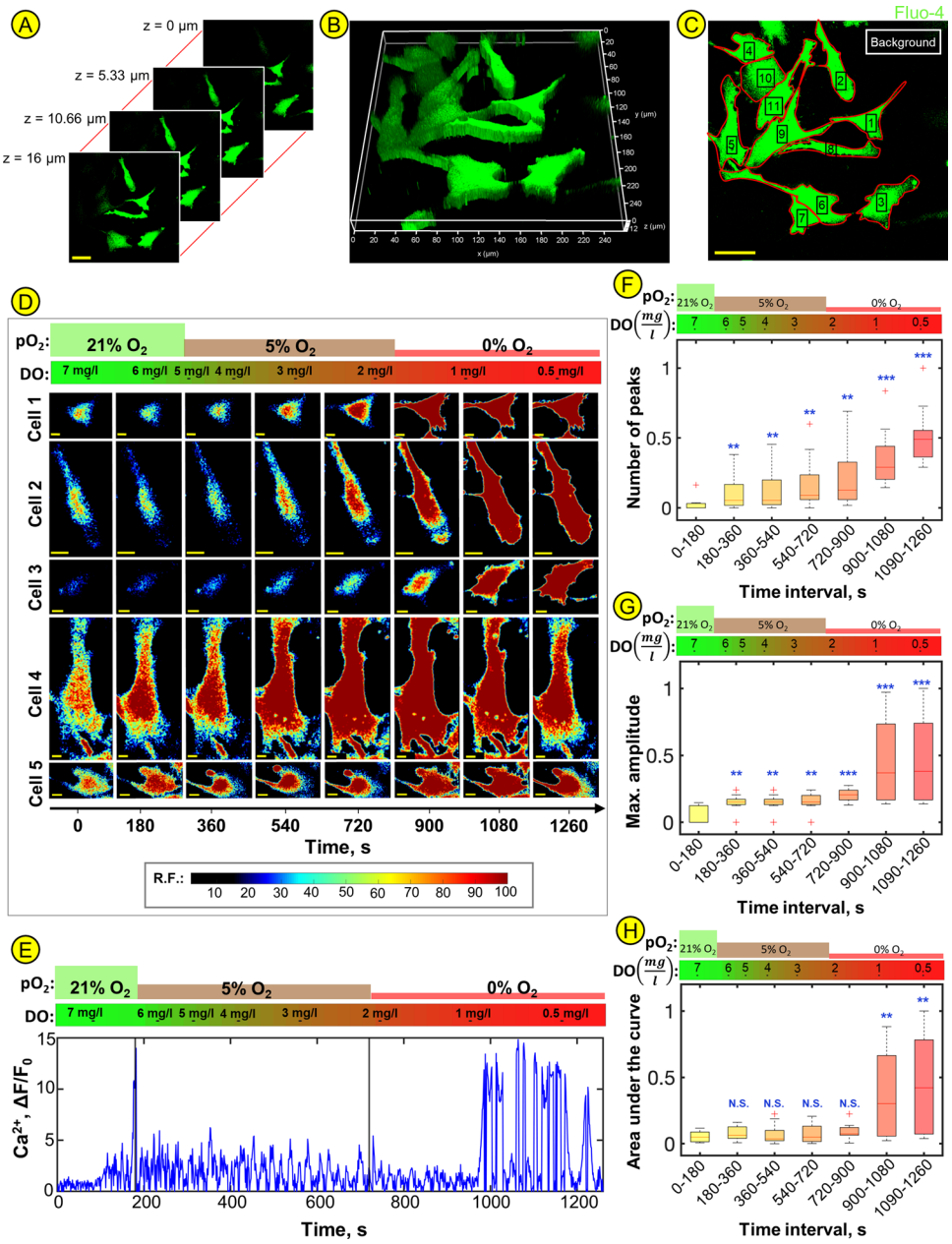

Figure 5. 3-D-time-lapse imaging of cytosolic Ca^{2+} in HMC-3 cells under a steep hypoxic gradient reveals the increase in Ca^{2+} amplitude and delay in recovery at 0% O_2 environments. (A) Representative images of cells were captured across four different focal planes to obtain the volumetric intensity profile of Fluo-4. (B) 3-D rendering was performed from the serial-cross-sectional images captured at a representative time instance. (C) ROIs are drawn around the cells after dimension reduction to extract mean intensity values (scale bar = 50 μm). (D) Intensity map of the Ca^{2+} spiking profile for five representative cells upon treatment with 21, 5, and 0% O_2 environments sequentially at indicated time points (scale bar = 10 μm). The images are obtained by dimension reduction of 3-D stacks to provide maximum intensity projections. The O_2-partial pressure (pO_2) and DO values indicate the severity of hypoxia at different time points. (E) Time-lapse of Fluo-4 intensity captured from a single representative cell. Intensity values have been normalized to show the fold change increase in cytosolic Ca^{2+} when sequentially subjected to 21, 5, and 0% O_2 environments. Box plot representation of the features of Ca^{2+} oscillations in different time windows corresponding to time-dependent hypoxic gradient: (F) number of peaks, (G) maximum amplitude, and (H) area under the curve (number of cells = 11, $p < 0.05$(*), $p < 0.01$(**), $p < 0.001$(***), and $p > 0.5$ (N.S.—no significance), one-way Kruskal Wallis test).

signaling pathways during ischemic shock (Supplementary Figure S5).

2.2. Effect of the Acute Hypoxic Gradient on Cell-State Markers. *2.2.1. Cellular Hypoxia Leads to Increased Amplitude and Frequency of Cytosolic Ca^{2+} Oscillations.* Since cytosolic Ca^{2+} plays a governing role in cellular functionality and assumes the molecular basis of cell state, we first investigated whether the steep gradient of hypoxia induces any change in the spiking pattern of cytosolic Ca^{2+} concentration. Figure 5A shows the 3-D-sectioning at a representative time instance. The cross-sectional imaging performed at different focal planes, enabled us to obtain volumetric Ca^{2+} values (Figure 5B). Since hypoxic conditions lead to cell migration and shrinkage, 3-D imaging in LSCM is expected to provide more accurate results than conventional two-dimensional (2-D) imaging (Supplementary Figure S6).

https://doi.org/10.1021/acschemneuro.2c00807
ACS Chem. Neurosci. 2023, 14, 1810−1825

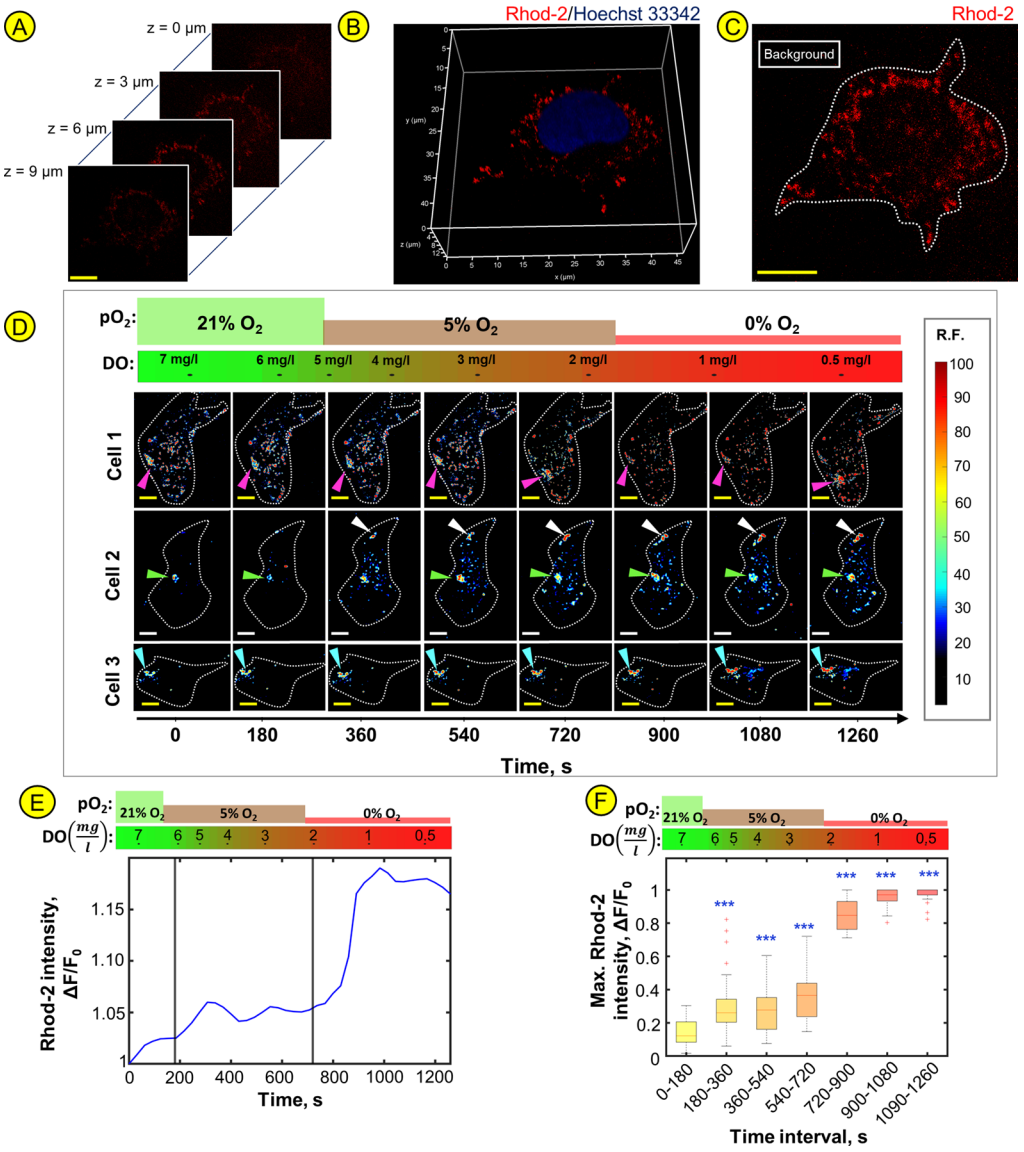

Figure 6. 3-D-time-lapse imaging of mitochondrial Ca^{2+} in HMC-3 cells under hypoxic gradient reveals the mitochondrial Ca^{2+} overload in 0% O_2 environment. (A) Representative images of single-cell captured across four different focal planes to obtain volumetric intensity profile of Rhod-2. (B) Positioning of the 3-D mitochondrial network around the nucleus (stained with Hoechst 33342). The Rhod-2AM labeling allows the detection of mitochondrial Ca^{2+} levels. (C) Dimension reduction of the image stack to extract mean intensity values. (D) Intensity map of the time-lapse images acquired via LSCM of three representative cells shows an overload in mitochondrial Ca^{2+} levels upon treatment with 21, 5, and 0% O_2 environments sequentially, at indicated time points (scale bar = 10 μm). (E) Normalized Rhod-2 fluorescence intensity time-lapse for a single representative cell. (F) Box plot representation of maximum Rhod-2 intensity captured in different time windows corresponding to time-dependent hypoxic gradient (number of cells = 30, $p < 0.05$(*), $p < 0.01$(**), $p < 0.001$(***), and $p > 0.5$ (N.S.—no significance), one-way Kruskal Wallis test).

The merge of individual cross-section planes obtained after dimension reduction around the cell peripheries is shown in Figure 5C. The time-lapse of fluorescence intensity clearly shows the increase of cytosolic Ca^{2+} levels at a 5% O_2 environment compared to the basal level Ca^{2+} oscillations (Figure 5D). Specifically, such pulsatile behavior indicates a delayed recovery of Ca^{2+} transients (Figure 5E and Supplementary Video S6).

Upon quantification of the imaging data, we observed an increase in the frequency of Ca^{2+} spiking at a 5% O_2 environment (Figure 5F), followed by an increase in both frequency and amplitude of oscillations at a 0% O_2 environment (Figure 5G,H). Furthermore, the spiking pattern at a 0% O_2 environment showed up to a 10-fold increase in the amplitude values (Figure 5E). Interestingly, after 250−300 s of exposure to a 0% O_2 environment, the cells also show a delayed recovery in the Ca^{2+} spiking profiles.

To compress the rich information observed in these time-resolved profiles into a means of comparing conditions, we performed feature-based *k*-means clustering.[41] Based on the DB-index values, four clusters were observed in this data set (Supplementary Figure S7A−D). Each cluster corresponds to the activity state of the individual cells.[42] It can be observed from Supplementary Figure S7D and S8 that as cells are exposed to hypoxic gradient, they change their state and transition to highly active states. After 180 s of 0% O_2 exposure, all cells transition to the clusters with cytosolic Ca^{2+} overload.

https://doi.org/10.1021/acschemneuro.2c00807
ACS Chem. Neurosci. 2023, 14, 1810−1825

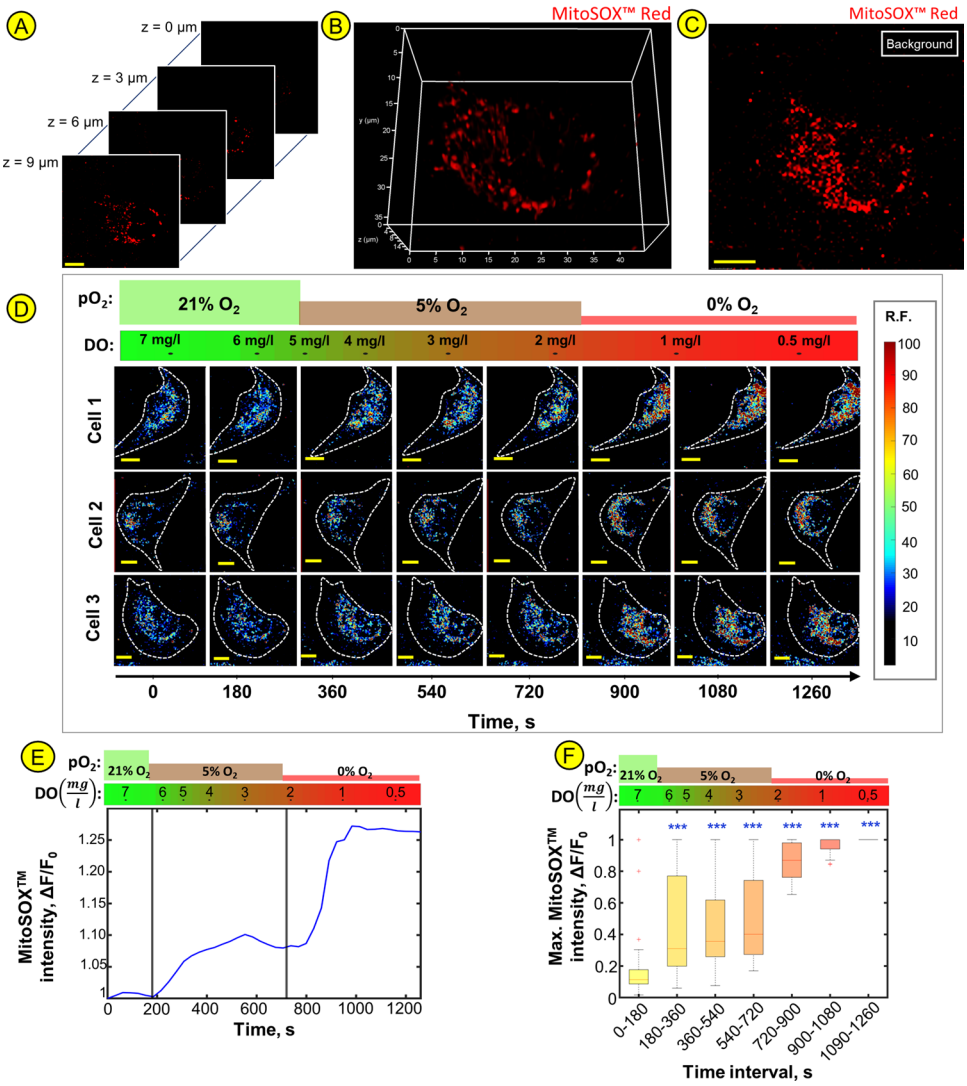

Figure 7. 3-D-time-lapse imaging of mitochondrial superoxide in HMC-3 cells under a hypoxic gradient reveals the increase in mitochondrial superoxide in 5 and 0% O_2 environments. (A) Representative images of single-cell captured across four different focal planes to obtain the volumetric intensity profile of MitoSOX Red. (B) Accumulation of mitochondrial superoxide inside the cell. (C) Dimension reduction of the image stack for extraction of mean intensity values. (D) MitoSOX fluorescence intensity levels in three representative cells showcase the increase in mitochondrial superoxide upon treatment with 5 and 0% O_2 environments sequentially, at indicated time points (scale bar = 10 μm). (E) Normalized MitoSOX Red fluorescence intensity-time-lapse for a single representative cell. (F) Box plot representation of maximum MitoSOX Red intensity captured in different time windows corresponding to time-dependent hypoxic gradient (number of cells = 30, $p < 0.05$(*), $p < 0.01$(**), $p < 0.001$(***), and $p > 0.5$ (N.S.—no significance), one-way Kruskal Wallis test).

2.2.2. Cellular Hypoxia Leads to Overload and Saturation in Mitochondrial Ca^{2+} Levels. Since the cytosolic Ca^{2+} overload and delayed recovery were apparent, we aim to investigate the dynamics in mitochondrial Ca^{2+} load and the correlation between time courses. In order to find this, we performed 3-D time-lapse imaging of mitochondrial Ca^{2+} imaging using the same hypoxic gradient as mentioned above (Figure 6A). The Rhod-2 indicator predominantly localizes in the mitochondrial filaments and highlights the dense mitochondrial network around the cell nucleus upon Ca^{2+} overload (Figure 6B). Similar to Fluo-4 quantification, the merge of individual cross-section planes obtained after dimension reduction (Figure 6C) was used to obtain the time-lapse of intensity values.

After staining the cells with Rhod-2 to detect the mitochondrial Ca^{2+}, the fluorescence intensity was generally weak in the control environment (21% O_2), as shown in Figure 6D. However, after hypoxia treatment, the characteristic localization of mitochondrial Ca^{2+} was observed gradually (Figure 6E,F and Supplementary Video S7). It can be noted that mitochondrial Ca^{2+} uptake occurs immediately in response to the cytosolic Ca^{2+} overload. An increase in the size of the mitochondrial network can also be observed in Figure 6D, suggesting mitochondrial swelling. High mitochondrial Ca^{2+} concentrations indicate the stress buildup in the mitochondria, which may further lead to ROS generation.[43]

2.2.3. Hypoxia Increased Mitochondrial Superoxide Production in the HMC-3 Cells. In order to investigate the consequences of mitochondrial Ca^{2+} overload, we assessed the intracellular dynamics of mitochondrial superoxide using the MitoSOX Red imaging assay (Figure 7A–C). Exposure of HMC-3 cells to the hypoxia gradient resulted in a significant increase in intracellular mitochondrial superoxide levels measured by MitoSOX fluorescence. As shown in Figure

https://doi.org/10.1021/acschemneuro.2c00807
ACS Chem. Neurosci. 2023, 14, 1810−1825

7D−F, switching the O_2 supply from 21 to 5% causes a marked increase in MitoSOX Red fluorescence. However, when the supply of O_2 was switched from 5 to 0% after 9 min, a drastic increment in the mitochondrial superoxide level was observed. Furthermore, as the O_2 supply was maintained at 0%, saturation in the mitochondrial superoxide levels was achieved (Supplementary Video S8). These results demonstrate the induction of hypoxic responses and the upregulation of intracellular mitochondrial superoxide in HMC-3 cells. Overall, the results show that induction of a hypoxic gradient results in a delay in Ca^{2+} recovery followed by mitochondrial Ca^{2+} overload and mitochondrial superoxide generation within 18 min. However, cell death is minimal in this time frame (Supplementary Figure S5).

Comparing the dynamics of cytosolic Ca^{2+}, mitochondrial Ca^{2+}, and mitochondrial superoxide together (Figure 8 and Supplementary Figure S9), it can be seen that the frequency and amplitude of oscillation in cytosolic Ca^{2+} increase upon the induction of acute hypoxic shock. There is an immediate increase in mitochondrial Ca^{2+} and mitochondrial superoxide production, suggesting a positive feedback of cytosolic Ca^{2+} on mitochondrial Ca^{2+} and mitochondrial superoxide. On the other hand, as the mitochondrial superoxide levels increase, there is a 10-fold increase in the amplitude of cytosolic Ca^{2+} oscillation, suggesting that mitochondrial superoxide production adds to the hypoxic injury. Based on these results, it can be inferred that cytosolic-Ca^{2+} is an early marker of stroke.

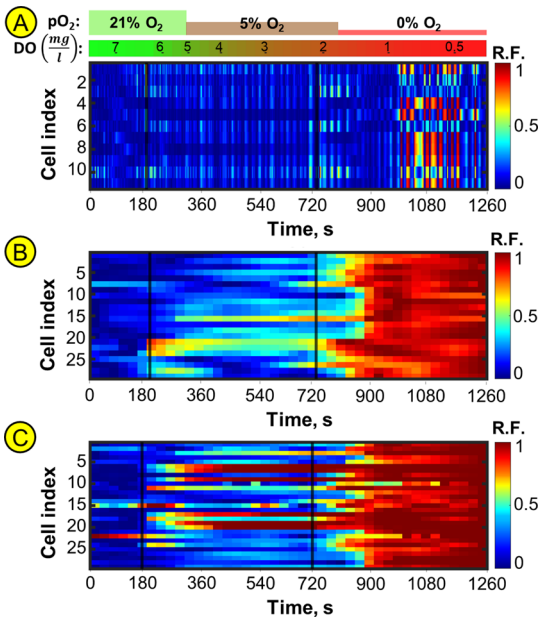

Figure 8. Comparison of population-level time-lapse traces reveals the correlation between cellular Ca^{2+} level and mitochondrial superoxide generation under acute hypoxia-induced in 21 min. Heat map representation of (A) cytosolic Ca^{2+}, (B) mitochondrial Ca^{2+}, and (C) mitochondrial superoxide in the HMC-3 population.

2.3. Application of the Ischemic Model: Comparison of Reoxygenation and Efficacy of the Calcium Channel Blocker on Hypoxia-Treated Cells. To validate the hypoxia model, we next demonstrated the applicability to allow the comparison of the L-type CCB (nifedipine) on a test case of ischemia (0% O_2 environment for 1 h) that can happen in a stroke.[20] The protective effect of nifedipine was compared with reoxygenation. This study assumes clinical importance in the context of infeasibility in reoxygenation at the ischemic onset in a timely manner. The design of the experiment, including control and hypoxia treatment cases, is given in Figure 9A.

The results show that there is a significant improvement in cell viability compared to hypoxic conditions (case 3) when nifedipine is used as the drug (case 4) ($p < 0.05$) (Figure 9B). Additionally, there is no significant difference in cell viability for nifedipine treatment for the control case ($p > 0.05$ for control-21% O_2 (case 1) and control-21% O_2 + Nif (case 2)), indicating that the 4 μM dose of nifedipine has no toxic effect in the experimental time frame. While comparing reoxygenation with nifedipine, we found that reoxygenation (case 5) provides better protection than nifedipine treatment (case 4) ($p < 0.05$). However, there is no significant difference between "reoxygenation + nifedipine treatment" (case 6) and reoxygenation (case 5). Hence, it can be concluded that nifedipine is able to protect the cells within 30 min of treatment time. Overall, the results show the potential for nifedipine to be used as a drug under hypoxic conditions at ischemia onset, with no adverse effects on the cellular level. Nifedipine may achieve increased cell survival before definitive reoxygenation therapies can be instituted. However, there is no synergistic effect between nifedipine and reoxygenation within the time scale considered in this study, which can be attributed to the fact that the role of nifedipine is only restricted to reducing ischemia-induced cell damage.

Next, we assessed the cytosolic Ca^{2+} levels for the six cases stated in Figure 9A. The bar plot of mean Fluo-4 fluorescence intensities ± SEM for the six cases after one-hour treatment is shown in Figure 9C. It can be observed that 1 hour of exposure to a 0% O_2 environment (case 3) leads to an over a four-fold increase in cytosolic Ca^{2+} levels. While the treatment with 4 μM nifedipine under hypoxia (case 4) causes a significant decrease in the cytosolic Ca^{2+} levels ($p < 0.01$), reoxygenation (case 5) has a superior effect on lowering the cytosolic Ca^{2+} levels ($p < 0.01$). It is observed that there is no significant difference in the Ca^{2+} level reduction in the case of "reoxygenation + nifedipine treatment" (case 6) and "reoxygenation treatment" (case 5) as found while evaluating the cell viability.

Next, we also test if the drug treatment can modulate the gene expression levels along with the reduction of Ca^{2+} levels within a short span of 60 min. For this, we compare the protective effect of reoxygenation and drug treatment by investigating the expression of *HIF1A*[12] and *OXR1*[12] genes within the same time scale. The qRT-PCR results show a 16.50-fold change in *HIF1A* expression and a 201.21-fold change in *OXR1* expression in cells incubated in 0% O_2 for 60 min (case 3), indicating induction of significant oxidative stress in the cells in the absence of any intervention. All the interventions studied in this work, treatment with nifedipine in the midst of hypoxia (case 4), reoxygenation after half an hour of hypoxia (case 5), and reoxygenation along with nifedipine treatment (case 6) show a significant reduction in the expression of *HIF1A* ($p < 0.05$) and *OXR1* ($p < 0.05$) (Figure 9D,E). Among the three different interventions studied here, there is no statistically significant difference in the expression of *HIF1A* (Figure 9D) and *OXR1* (Figure 9E). The results indicate that the nonprophylactic treatment with nifedipine is comparable to reoxygenation with respect to the protection from oxidative stress within 30 min of treatment.

https://doi.org/10.1021/acschemneuro.2c00807
ACS Chem. Neurosci. 2023, 14, 1810−1825

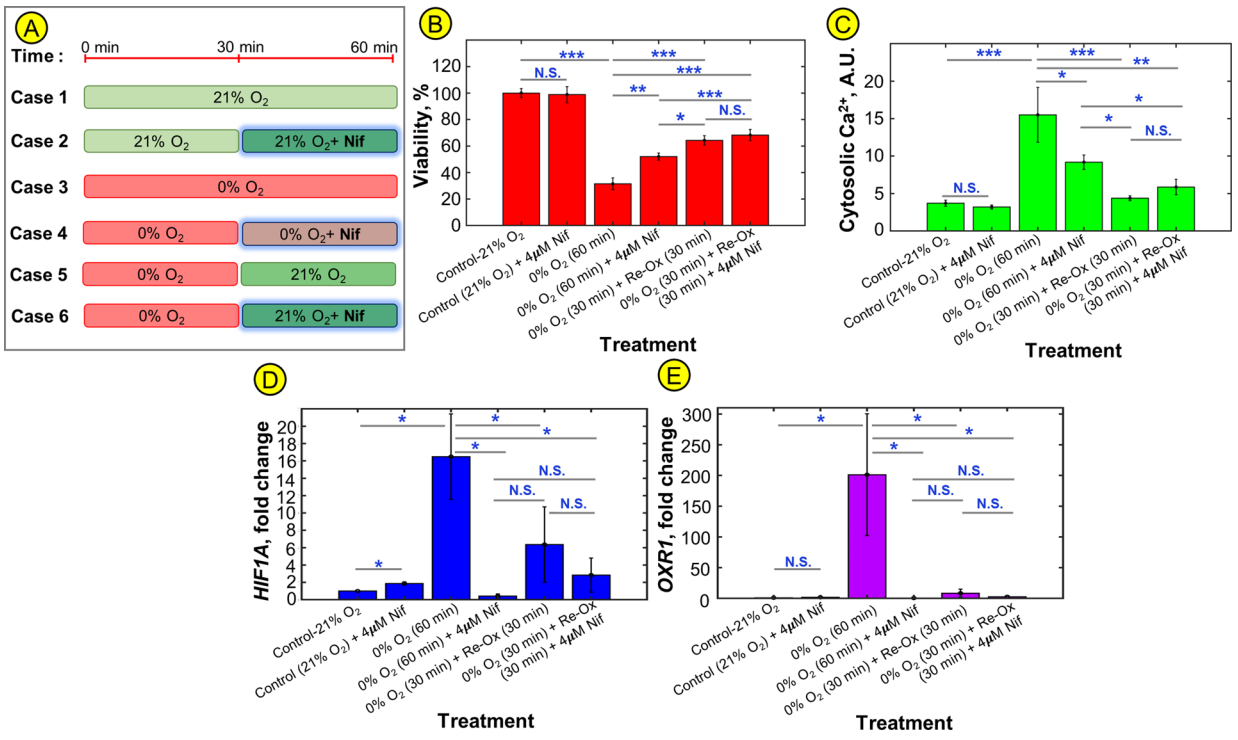

Figure 9. Validation of hypoxia model through comparison of reoxygenation and L-type CCB. (A) Design of experiments for the study of reoxygenation and Nifedipine (Nif.) treatment. Case 1: "21% O_2 for 60 min", Case 2: "21% O_2 for 60 min + 4 μM Nif. added at 30 min," Case 3: "0% O_2 for 60 min," Case 4: "0% O_2 for 60 min + 4 μM Nif. added at 30 min," Case 5: "0% O_2 for 30 min + 21% O_2 for 30 min," Case 5: "0% O_2 for 30 min + 4 μM Nif. added at 30 min + 21% O_2 for 30 min." Bar plot representation of (B) Cell viability at different treatment combinations. (C) Mean fluorescence intensities of Fluo-4 staining in HMC-3 cells (n = 30). (D) Fold change of *HIF1A* expression at different treatment combinations. (E) Fold change of *OXR1* expression at different treatment combinations. All the graphs are representatives of biological triplicates. β-Actin was used as the normalization control for qRT-PCR ($p < 0.05$(*), $p < 0.01$(**), $p < 0.001$(***), and $p > 0.5$ (N.S.—no significance), one-way Kruskal Wallis test).

Considering the results of cell viability, cytosolic Ca^{2+}, and gene expression together, it can be interpreted that in the case of hypoxic injury (case 3), Ca^{2+} overloading (Figure 9C) leads to overexpression of hypoxia markers and consequent reduction in cell viability (Figure 9B). All three treatments considered in this work, nifedipine treatment (case 4), reoxygenation (case 5), and "reoxygenation + nifedipine treatment" (case 6), alleviate the symptoms of hypoxia by significantly lowering the Ca^{2+} levels (Figure 9C) and oxidative stress (Figure 9D,E).

To test the generality of the proposed method, we performed a cell viability assay under hypoxic stress on the Neuro-2a (N2a) cell line. Specifically, the N2a cells were chosen for this study, as the overexpression of L-type VGCCs under hypoxic stress has been observed for these cells.[44] Following the same protocol used for the microglia cell line, we exposed N2a cells to acute hypoxia and assessed cell viability. It can be observed that compared to HMC-3 cells, N2a cells are less sensitive to hypoxic stress (Figure 10A and Supplementary Figure S10), and a significant reduction in viability is found at 3−4 h. Hence, we propose an updated design to compare the reoxygenation and nifedipine-mediated recovery of N2a cells (Figure 10B). Here, the N2a cells were exposed to 3.5 h of hypoxia followed by 0.5 h of treatment with reoxygenation, nifedipine, or both. Similar to the microglia cell line study, the results show that there is a significant improvement in the viability of N2a cells with nifedipine treatment (case 4) as compared to hypoxic conditions (case 3) ($p < 0.05$) (Figure 10C). Moreover, reoxygenation (case 5) provides better protection than nifedipine treatment (case 4) ($p < 0.05$) in N2a cells, and there is no significant difference between "reoxygenation + nifedipine treatment" (case 6) and reoxygenation alone (case 5). Together, these results indicate that CCBs can protect both microglia and neuron cells in CNS from ischemic stroke.

3. DISCUSSION

Visualization of intracellular dynamics under acute hypoxic shock can play a key role in designing therapeutics against stoke. While the $CoCl_2$-based hypoxia model is popularly used for dose-dependent stabilization of HIF, it is unsuitable for obtaining dynamic information on redox pathways under acute hypoxic stress and their recovery time while testing the protectivity of drugs within a short period. To overcome these issues, we used the chamber-based hypoxia setup attached to a high-resolution imaging system that can be used for testing drugs along with reoxygenation. The novelty of this setup is its ability to administer acute hypoxia and real-time control of O_2 levels, which permits the mimicking of stroke-like conditions.

The first two objectives demonstrate a protocol for in situ live-cell confocal imaging of cell morphology, cytosolic Ca^{2+}, mitochondrial Ca^{2+}, and mitochondrial superoxide under an acute gradient of hypoxia in HMC-3 microglia cells. Our approach is based on LSCM-3-D time-lapse imaging/analyses of the whole cell. While 2-D analyses provide details from an optical cross-section of the cell, 3-D reconstruction, accomplished by taking a stack of serial slices throughout the cell

https://doi.org/10.1021/acschemneuro.2c00807
ACS Chem. Neurosci. 2023, 14, 1810−1825

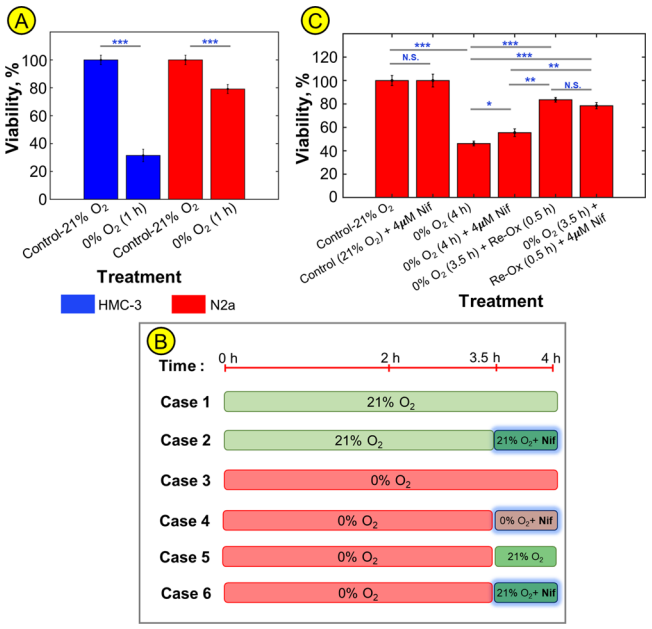

Figure 10. Assessment of generality of the experimental setup using N2a cell line. (A) Bar plot comparison of the viability of HMC-3 and N2a cells under acute hypoxia (0% O_2) for a duration of 1 h. (B) Design of experiments for the study of reoxygenation and Nifedipine (Nif.) treatment in N2a cells. Case 1: "21% O_2 for 4 h," Case 2: "21% O_2 for 4 h + 4 μM Nif. added at 3.5 h", Case 3: "0% O_2 for 4 h," Case 4: "0% O_2 for 4 h + 4 μM Nif. added at 3.5 h", Case 5: "0% O_2 for 3.5 h + 21% O_2 for 30 min," Case 5: "0% O_2 for 3.5 h + 4 μM Nif. added at 3.5 h + 21% O_2 for 30 min". (C) Bar plot representation of cell viability at different treatment combinations ($p < 0.05$(*), $p < 0.01$(**), $p < 0.001$(***), and $p > 0.5$ (N.S.—no significance), one-way Kruskal Wallis test).

volume, yields a volumetric signal that is more accurate than 2-D imaging (Supplementary Figure S6).

In the first two sections of this paper, we have also studied the hypoxia-injury-hallmarks during the induction of a steep temporal gradient of acute hypoxia in cells. To complement the experimental workflow, we incorporated semiautomated image analysis and feature extraction from the confocal videos. The clustering-based cell-state classification enables quantitative analysis of cytosolic Ca^{2+}. We also implemented image segmentation and 3-D rendering of the cell nucleus to quantify chromatin condensation. This enabled us to study nuclear morphology from the migrating cells, giving a more accurate analysis of confocal videos. Overall, this analysis pipeline permits robust multidimensional quantification of cell states and Ca^{2+} dynamics that provides a valuable resource to accelerate research in understanding cellular response to stroke. Since mitochondrial superoxide is a key inducer of cellular apoptosis,[45] the model was further investigated using the dynamic measurement of mitochondrial superoxide. The data suggest that mitochondrial superoxide and cytosolic/mitochondrial Ca^{2+} signals are intimately interconnected, leading to a specific and adaptive response to ischemic shock. Acute ischemic shock leads to elevated frequency and amplitude of cytosolic Ca^{2+}, which contributes to mitochondrial Ca^{2+} overload. Elevated mitochondrial Ca^{2+} may trigger the production of mitochondrial superoxide, possibly because of the stimulation of respiratory chain activity.[46] Such changes in the Ca^{2+} homeostasis and mitochondrial superoxide levels can be taken as a model for stroke. Supplementary Figure S11 shows the schematic of a plausible molecular pathway upon induction of hypoxic stress and the progression of Ca^{2+} overload and mitochondrial superoxide generation.

After studying the dynamics of molecular markers under hypoxia, cytosolic Ca^{2+} was identified as an early marker that further leads to mitochondrial Ca^{2+} overload and superoxide generation. In the third objective, we demonstrated the capability of the hypoxia model to test drug efficacy. Here, we studied the effect of nifedipine treatment, reoxygenation, and "reoxygenation + nifedipine treatment" using imaging and gene expression studies. Although nifedipine has been used to protect cells through Nrf2 translocation under long-term hypoxic conditions with prophylactic treatment,[19] whether the CCB can be used nonprophylactically to protect molecules in a shorter time scale is not known. In the current study, we compared the drug efficacy to reoxygenation in the case of nonprophylactic intervention.

We found that although nifedipine treatment has lower cell viability than reoxygenation or "reoxygenation + nifedipine treatment," it shows significant improvement in cell health over the untreated case, making it a suitable option for hypoxia intervention when reoxygenation is not possible immediately. It is known that the peripheral areas of the cerebral tissue in the ischemic area, the ischemic penumbra, go through gradual apoptosis following an ischemic stroke, while the central areas are subject to necrotic changes. These peripheral parts, which are the target areas for salvage with revascularization therapy, can potentially have increased viability through the anti-apoptotic effect mentioned above after an ischemic stroke.[47,48] No significant difference between reoxygenation and "reoxygenation + nifedipine treatment" in terms of viability and gene expression indicates no plausible synergistic effect on reoxygenation and nifedipine within studies the duration of 1 h. However, given that the proportion of viable cells is higher if treated with nifedipine under anoxic conditions, reoxygenation therapy can potentially have higher chances of salvaging more cells if the ischemic penumbra is exposed to nifedipine during the period of anoxia. Therefore, it is possible that nifedipine can be administered to a patient in the immediate aftermath of an ischemic stroke when the treatment can be followed by intravascular or systemic revascularization strategies.[49] Further long-term experiments can be designed to examine the synergistic effect between the drug and reoxygenation.

Although the use of nifedipine assumes clinical significance in the context of ischemia, it should be noted that nifedipine is known to lower blood pressure at a certain dose range,[50] which can, in turn, reduce cerebral perfusion pressure, resulting in reduced O_2 delivery to the tissues. Therefore, the outcome of nifedipine use will be a combination of its effect on the preservation of cell viability and the lowering of cerebral perfusion pressure. Further animal studies need to be performed to determine the optimum systemic dose to achieve a cell-preserving effect so that it is ensured that a higher number of neural cells are going into the revascularization treatment.

The viability and Ca^{2+} imaging results obtained from live-cell imaging portray the outcome of cell-signaling processes under stroke and correlate well with the predictions from gene expression. Since live-cell Ca^{2+} imaging results conform with the gene expression experiments and provide immediate results, Ca^{2+} imaging can directly be used as a powerful tool for drug screening.

https://doi.org/10.1021/acschemneuro.2c00807
ACS Chem. Neurosci. 2023, 14, 1810−1825

Additional studies on N2a cells suggest that our original observations of acute hypoxia-induced cell death in microglia cells may be a generalizable phenomenon in other cell types. Thus, we conjecture that the setup can be used to develop and test therapeutics against pathological conditions related to acute hypoxia in other cell lines. Specifically, the real-time control of O_2 and drug delivery can be further used to understand the cell states and dynamic molecular signatures upon drug treatment.

Since the partial pressure of O_2 was controlled to modulate the DO in cell culture media, there is a lag between the set point of the controller and DO. In the future, to mimic the conditions of acute stroke accurately, it is critical to establish an optimized perfusion system with the capability of rapid exchange of the solution bathing with the cell culture system.[22] However, it is rather challenging to establish such a perfusion system coupled with confocal imaging, while numerous conditions need to be assessed for drug testing. Although this perfusion system provides better control over the hypoxic conditions, the proposed setup with a Petri dish allows us to perform multiple experiments that are necessary for controlling several conditions, including drug treatment and reoxygenation. Progressive hypoxia can also be achieved via the perfusion of O_2-deprived media in the microfluidic chip.[13] Another limitation of this study is that long-term imaging is challenging with fluorescent dyes as they are susceptible to photobleaching. Additionally, fluorophores may impose toxicity on the cells. Although the current work is based on a short-term study, the long-term effect of drug testing could provide better applicability to this model. In the future, the use of genetically encoded sensors[51] can be used for long-term Ca^{2+} imaging. The other limitation of the study is the use of continuous excitation with lasers that may provide phototoxicity to the live cells. Minimizing laser power and using hybrid detectors to capture the emission alleviated this issue. Moreover, monitoring multiple fluoroprobes simultaneously was not possible since the internalization time and incubation temperature for different indicators were different. Also, the emission ranges of several fluoroprobes used together lead to crosstalk between signals. To eliminate the effect of crosstalk between different fluoroprobes, we conducted cytosolic Ca^{2+}, mitochondrial Ca^{2+}, and mitochondrial superoxide imaging separately.

Furthermore, an inflammatory process and nitric oxide generation are associated with cellular ischemia, and these processes are not replicated within our experiment. Since hypoxia is also known to affect the pH of the culture media,[23,52] further experiments may be performed to study the pH changes during ischemic stroke. Animal model studies may also address the influence of immune-ischemia interaction and vasoregulatory mechanisms underlying nifedipine.[53,54]

4. CONCLUSIONS

This work focuses on developing an experimental model to study the effect of acute hypoxic shock in the microglia cell line by 3-D imaging using LSCM. The proposed ischemic shock model with real-time control in hypoxia is able to mimic the immediate oxidative stress and reveals the time course of signaling events, Ca^{2+}, and mitochondrial superoxide in situ, along with chromatin condensation and cell death. We found that 3-D imaging is crucial in the context of acute hypoxia since the hypoxic insult leads to a change in cell shape and location in the z-direction. Our results elucidate that cytosolic Ca^{2+}, mitochondrial Ca^{2+}, and superoxide are the immediate pivotal hallmarks of cell state under ischemic shock. Hence, these molecules can be targeted for designing drugs that can address severe hypoxic insults in the CNS within a shorter window of time. To demonstrate the applicability of our hypoxia model, we showed that the model is able to compare the efficacy of a CCB and reoxygenation in a case study of stroke. Along with the 3-D time-lapse imaging of molecular markers of hypoxia, we have also demonstrated that the setup is able to decipher the immediate change in gene expression through RT-PCR experiments. Furthermore, we show that the same experimental setup can be used to test neuronal cell drugs. The generality of the method is explored in N2a cells. In both HMC-3 and N2a cells, the CCB is comparable to reoxygenation. Taken together, our results indicate a plausible application of CCBs as an emergency drug for stroke. Therefore, testing these drugs in future animal models may further elucidate the significance in comparison to reoxygenation.

5. MATERIALS AND METHODS

5.1. Reagents. Dulbecco's modified Eagle's medium (DMEM) was purchased from GE Healthcare Life Sciences, US. Fetal bovine serum (FBS), penicillin−streptomycin solution, L-glutamine, 0.25% (w/v) trypsin-0.53 mM, Hanks' Balanced Salt Solution (HBSS) (with Ca^{2+} and Mg^{2+}, no phenol red), phosphate-buffered saline (PBS) (1×), Hoechst 33342, Trihydrochloride Trihydrate, Fluo-4 AM, MitoSOX Red Mitochondrial Superoxide Indicator, propidium iodide, and Rhod-2 AM were purchased from Gibco, Life Technology, US.

5.2. Cell Culture. HMC-3 cells were supplied by L V Prasad Eye Institute, Hyderabad, India. Mouse Neuro-2a (N2a) neuroblastoma cells were purchased from the National Centre of Cell Science Pune (NCCS, Pune, GSM1351). Both HMC-3 and N2a cells were grown in DMEM supplemented with 10% FBS, 100 units/mL penicillin, 100 μg/mL streptomycin, and 2 mM L-glutamine. Cells were cultured in different T-25 flasks (Corning, US). The cultures were maintained in a humidified 5% CO_2 atmosphere at 37 °C, with media replaced every second day and subcultivation at 80−90% confluence. The cell growth profile for HMC-3 cells is provided in Supplementary Figures S12 and S13.

For all the confocal video acquisitions, 1×10^5 cells were seeded in optical-bottom Petri dishes (dish size 35 mm and well size 10 mm) (Cellvis, US) and imaged 48 h after seeding. All the experiments were performed with culture-passage numbers under 10 to minimize the experimental variations.

5.3. Setup for Induction of Hypoxia and Live-Cell Imaging. The setup for live-cell imaging comprised an imaging chamber that was placed on top of the confocal microscope (TCS SP8, Leica, Germany) and retained within an incubator unit attached to the microscope (Figure 1A). The top of the imaging chamber was composed of quartz glass to allow optical transmission. The optical-bottom Petri dishes consisting of cells were placed in a small cavity at the center of the chamber's base. The sides were sealed to minimize contamination and deviation from the set hypoxic conditions. The imaging chamber was supplied with a humidified mixture of CO_2, O_2, and N_2 gases (flow rate 40 L/h). The CO_2 composition was fixed at 5%, and O_2 was varied from 21−0% to observe the effect of hypoxic stress. The gas-mixture composition and flow rate were controlled by a feed-forward controller, while the temperature controller was used to fix the incubation temperature at 37 °C. All the gases used in the study were cell culture grade and prefiltered using a Whatman filter. Movies were made using the 20×/0.7 dry and 40×/1.3 oil objectives. While the 20x objective was used for population imaging, the 40× objective was used for single-cell imaging.

To assess the DO level that can be achieved through the controller, we determined the time course of DO in the culture media after the induction of hypoxia. DO measurements were done by immersing the electronic hand-held O_2 meter (Oakton DO 700) in a 50 mL conical

https://doi.org/10.1021/acschemneuro.2c00807
ACS Chem. Neurosci. 2023, 14, 1810−1825

Table 1. Nucleotide Sequences of Primers Used in qRT-PCR

gene	primer sequence (forward)	primer sequence (reverse)
β-actin	5′-CATGTACGTTGCTATCCAGGC-3′	5′-CTCCTTAATGTCACGCACGAT-3′
HIF1A	5′-CCAGCAGACTCAAATACAAGAACC-3′	5′-TGTATGTGGGTAGGAGATGGAGAT-3′
OXR1	5′-CTGATGGTGATTAAAG ACAGTG-3′	5′-CACTTAAAGACCTCAAACTCC-3′

tube (Figure 4B). Since the direct insertion of O_2 probes may interfere with the cell responses, this setup was used to mimic the condition of the imaging experiments where cells are subjected to hypoxic gradients with time.

5.4. Cell Viability Assay. Hoechst 33342-propidium iodide staining was used to quantify cell death. Cells were incubated in the dark for 10 min with HBSS, containing 2.5×10^{-3} mg/mL Hoechst 33342 and 5×10^{-3} mg/mL propidium iodide. Since the objective of the experiment was to obtain the time-lapse monitoring of cell viability, and propidium iodide is cell impermeable, washing was not performed after incubation. This allowed in situ monitoring of cellular integrity. Sequential imaging was performed in the confocal microscope by exciting the cells with 405 nm (ultraviolet, 50 mW, direct modulation laser) and 561 nm lasers. The Hoechst 33342 emission was captured at ∼430−500 nm (blue), and the propidium iodide emission was captured at ∼600−650 nm (red). Cell viability was determined at each time instance as the viable cells were not permeable to propidium iodide.

We computed the viability of cells over time by performing morphological operations on blue (indicates all cells dead or alive) and red (indicates the dead cell) channels of each time frame (Supplementary Figure S14). In particular, at each instance, we extract blue and red channels from the image, convert them to a binary image, remove the spurious (or noise clusters) pixels, and then identify the connected components (cells). Next, for a chosen time frame, the number of components (cells) in the blue channel accounts for the number of live cells, and that in the red channel account for dead cells. Finally, we plot the number of cells (dead and alive) temporally.

The following MATLAB commands were used:

I. *bwareaopen*: to remove spurious points/pixels/regions.
II. *bwconncomp*: to identify connected components (or cell regions).

5.5. Imaging Cell Morphology. The morphological changes in the cell structure under the induction of hypoxia were observed using DIC imaging in confocal laser scanning microscopy. To eliminate any of the toxic effects of fluorescent indicator loading, morphological studies were performed without staining. Cells were tracked from the DIC-time-lapse videos manually using Fiji/ImageJ by tracking the movement of the centroid of the cell (Supplementary Figure S15).

5.6. Dynamic Cytosolic Ca^{2+} Imaging. The time-lapse of cytosolic Ca^{2+} was measured in terms of fold change in the intensity level of the Fluo-4 indicator. To stain the cells with Fluo-4, the growth medium was aspirated, and the cells were washed twice with HBSS. Thereafter, cells were incubated in the dark at 37 °C after adding 2 mL of HBSS containing 2 μM Fluo-4AM reagent for 30 min. After 30 min of staining, cells were rinsed twice with HBSS for 10 min each time.[55] Fluo-4AM was excited with 488 nm (blue), 40 mW, acousto-optical tunable filter (AOTF) argon laser, with emission collection in the range of ∼500−550 nm (green).[55] Different focal planes across the cell layer were imaged in order to obtain the volumetric-Ca^{2+} intensity.

5.7. Dynamic Mitochondrial Ca^{2+} Imaging. Similar to cytosolic Ca^{2+}, mitochondrial Ca^{2+} was measured as a fold change in the intensity level of the Rhod-2AM indicator. For Rhod-2 staining, cells were incubated in the dark at 4 °C after adding 2 mL of HBSS containing 0.5 μM Rhod-2AM reagent for 45 min. Incubation at low temperatures allows the minimization of subcellular compartmentalization, an inherent problem with the AM ester loading technique.[56] Before commencing fluorescence measurements, cells were washed with an indicator-free medium to remove any nonspecifically associated indicator. Incubation and washing with HBSS for a further 30 min (thrice, 10 min each time) allowed complete de-esterification of intracellular Rhod-2AM ester. Rhod-2 was excited with 561 nm (green), 20 mW, AOTF laser, with emission collection at ∼570−620 nm (red).

5.8. Mitochondrial Superoxide Imaging for Measurement of Cell Stress. Reactive O_2 species (ROS) are free radicals that accumulate in the cells under stressed conditions and cause damage to DNA, RNA, and proteins and may consequently lead to cell death. The time course of mitochondrial superoxide (O^{2-}) produced in the cells was quantified by using a MitoSOX Red Mitochondrial Superoxide Indicator kit. Cells were stained with 2 μM MitoSOX Red solution in HBSS for 15 min followed by washing thrice with HBSS for 10 min each time. MitoSOX Red selectively targets mitochondria and undergoes oxidation by superoxide to form a stable fluorescent compound. MitoSOX Red was excited with 561 nm (green), 20 mW, AOTF laser, with emission collection at ∼580−620 nm (red).

5.9. Image Analysis for Quantification of Cytosolic Ca^{2+}, Mitochondrial Ca^{2+}, and Mitochondrial Superoxide. All 3-D images were uniformly gamma corrected to adjust the intensity of the fluorescence, and the noisy pixels were removed via thresholding (Supplementary Figure S17). To quantify the fluorescence intensity of indicator dyes, Fluo-4, mitochondrial superoxide, and Rhod-2 from all z-stacks, individual stack images were first merged using LASX software. After superimposing all the z-stacks, compressed z-stack images corresponding to each time point were obtained, and regions of interest (ROIs) were drawn manually for each cell. To obtain fluorescence intensities corresponding to these ROIs, intensities from individual focal planes were summed across the entire sample thicknesses to result in $[F_{\text{measured}} = F_1 + F_2 + \ldots F_n]$, where F_i represents fluorescence intensity for the ROI obtained from each z-stack. Average areal fluorescence intensity was calculated for each ROI at each time instance. Similarly, the background fluorescence was obtained from a region that did not show any fluorescence. After background-subtraction denoising, a moving-average-based algorithm was implemented in MATLAB (Supplementary Figure S18).[41]

5.10. Quantitative Real-Time Reverse Transcription (qRT-PCR). Quantitative RT-PCR was done to characterize the expression of *HIF1A* and *OXR1* genes under hypoxia. In brief, the total RNA was extracted from the HMC-3 cells before and after the stress induction by the TRIzol method. A total RNA of 500 nanograms (ng) was reverse-transcribed into cDNA using a Verso cDNA Synthesis Kit (ThermoFisher Scientific, Catalog No. AB1453B) according to the manufacturer's protocol.

To quantify the average mRNA expression, we performed qRT-PCR on an Applied Biosystems 7900 HT system for a total reaction volume of 10 μL. The reaction mixture (10 μL) included iTaqTM Universal SYBR Green Supermix (BIO-RAD, Catalog No. 172-5121), 200 nM of primer, and cDNA. The relative measure of the target gene concentration (Ct) was calculated using software SDS 2.4. Analysis of gene expression changes was done using the $2^{-\Delta\Delta Ct}$ method. Statistical analyses were performed using $2^{-\Delta\Delta Ct} \pm$ SEM in three technical and biological replicates. The housekeeping gene β-actin was used as a normalizing control. The primer sequences used for qRT PCRs are given in Table 1.

5.11. Validation of the Hypoxia Model. The validation of the hypoxia model was performed by testing if the model can also be used to compare the protective effect of the drug with reoxygenation under a test case of stroke. We specifically chose nifedipine for this study as the antineuroinflammatory effect of nifedipine on microglia cells has also been shown in refs 23, 36. For this study, we applied 0% O_2 stress on cells for 30 min. After the end of 30 min of hypoxic stress, cells were subjected to four different treatments (1) reoxygenation, (2)

https://doi.org/10.1021/acschemneuro.2c00807
ACS Chem. Neurosci. 2023, 14, 1810−1825

nifedipine treatment, (3) reoxygenation + nifedipine treatment, or (4) continued with a 0% O_2 environment for another 30 min. Based on the toxicity study shown in Supplementary Figure S19, a 4 μM dose of nifedipine was given to the cells. Control conditions were obtained through the maintenance of a 21% O_2 environment. The effect of nifedipine was also tested in the control cells with a 21% O_2 environment.

■ ASSOCIATED CONTENT

Supporting Information

The Supporting Information is available free of charge at https://pubs.acs.org/doi/10.1021/acschemneuro.2c00807.

Supplementary Video S1: time-lapse of cell viability under 21, 5, and 0% O_2 (MP4)
Supplementary Video S2: DIC time-lapse videos of cell populations under 21, 5, and 0% O_2 (MP4)
Supplementary Video S3: DIC time-lapse videos of three representative single cells for monitoring migration at 21% O_2 (MP4)
Supplementary Video S4: DIC time-lapse videos of three representative single cells for monitoring migration at 5% O_2 (MP4)
Supplementary Video S5: DIC time-lapse videos of three representative single cells for monitoring migration at 0% O_2 (MP4)
Supplementary Video S6: time-lapse of cytosolic calcium under a steep gradient of O_2 (MP4)
Supplementary Video S7: time-lapse of mitochondrial calcium under a steep gradient of O_2 (MP4)
Supplementary Video S8: time-lapse of mitochondria superoxide under a steep gradient of O_2 (MP4)
Protocol for imaging nucleus condensation; details of clustering algorithm to determine cell state; literature survey of acute hypoxia models reported for microglia cells (2010−2022); details of imaging parameters for 3-D imaging of cell viability, nuclear morphology, cytosolic Ca^{2+}, mitochondrial Ca^{2+}, and mitochondrial superoxide levels; 3-D imaging and volumetric quantification of nuclear condensation under hypoxia; effect of acute hypoxia on population morphology; cell division observed under 5% O_2; quantification of cell migration; viability under a steep gradient of hypoxia; comparison of Ca^{2+} imaging performed using a fluorescence microscope and LSCM; quantification and clustering of Ca^{2+} spiking behavior; clustering of principal component of mitochondrial Ca^{2+} and superoxide dynamics; schematic diagram of the molecular pathway for the proposed mechanism; cell proliferation profiles at 21, 2, and 1% O_2 environments; algorithm for automated detection of cell viability from the time-lapse videos; estimation of cell centroid using Fiji/ImageJ software; algorithm for segmentation of nucleus surface area and volume via *k*-means clustering; image tuning in the Leica LAS X software; moving-average-based algorithm for baseline correction; toxicity analysis of different doses of nifedipine via Hoechst 33342-PI assay (PDF)

■ AUTHOR INFORMATION

Corresponding Author

Lopamudra Giri − *Bioimaging and Data Analysis Lab, Department of Chemical Engineering, Indian Institute of Technology Hyderabad, Sangareddy, Telangana 502205, India;* orcid.org/0000-0002-3099-9068; Email: giril@che.iith.ac.in

Authors

Vaibhav Dhyani − *Bioimaging and Data Analysis Lab, Department of Chemical Engineering, Indian Institute of Technology Hyderabad, Sangareddy, Telangana 502205, India; Optical Science Centre, Faculty of Science, Engineering & Technology, Swinburne University of Technology, Melbourne, Victoria 3122, Australia;* orcid.org/0000-0002-0735-6937

Saurabh Kumar − *L V Prasad Eye Institute, Hyderabad, Telangana 500034, India; Manipal Academy of Higher Education, Manipal, Karnataka 576104, India;* orcid.org/0000-0002-6929-0830

Shanmukh Reddy Manne − *Department of Electrical Engineering, Indian Institute of Technology Hyderabad, Sangareddy, Telangana 502205, India*

Inderjeet Kaur − *L V Prasad Eye Institute, Hyderabad, Telangana 500034, India*

Soumya Jana − *Department of Electrical Engineering, Indian Institute of Technology Hyderabad, Sangareddy, Telangana 502205, India*

Sarah Russell − *Optical Science Centre, Faculty of Science, Engineering & Technology, Swinburne University of Technology, Melbourne, Victoria 3122, Australia; Peter MacCallum Cancer Centre, Melbourne, Victoria 3000, Australia; Sir Peter MacCallum Department of Oncology, The University of Melbourne, Melbourne, Victoria 3010, Australia*

Rahuldeb Sarkar − *Department of Respiratory Medicine and Critical Care, Medway NHS Foundation Trust, Gillingham, Kent ME7 5NY, U.K.; Faculty of Life Sciences, King's College London, London WC2R 2LS, U.K.*

Complete contact information is available at: https://pubs.acs.org/10.1021/acschemneuro.2c00807

Author Contributions

All authors contributed to the conception and design of the work. V.D., R.S., and L.G. planned the work. V.D. performed the hypoxia experiments and live-cell imaging. S.K. did the qRT-PCR for gene expression. S.R.M. and S.J. developed the algorithms for image segmentation. V.D., S.K., S.R.M., R.S., and L.G. contributed to the writing of the manuscript. V.D. prepared the schematics and figures. I.K., S.J., S.R., R.S., and L.G. reviewed the manuscript. All authors read and approved the final manuscript.

Notes

The authors declare no competing financial interest.

■ ACKNOWLEDGMENTS

The authors would like to thank the Director, Indian Institute of Technology Hyderabad (IIT-H), India, for his support and encouragement in performing this study. The authors acknowledge the research facilities provided by IIT-H, India. The authors also thank Dr. Saptarshi Majumdar, Dr. Kishalay Mitra, and Dr. Parag D. Pawar for their valuable feedback. Vaibhav Dhyani and Saurabh Kumar acknowledge fellowship support from MHRD and DBT (DBT/2020/LVPEI/1365), respectively. The authors also thank the Department of Biotechnology (DBT), India, for providing financial assistance in the form of the projects BT/PR22239/NNT/28/1269/

2017, BT/PR26978/NNT/28/1511/2017, and BT/PR32404/MED/30/2136/2019, and the Department of Science and Technology—Science and Engineering Research Board (DST-SERB), Ministry of Science and Technology, Government of India for the project EMR/2016/007068.

REFERENCES

(1) Holloway, P. M.; Gavins, F. N. E. Modeling Ischemic Stroke In Vitro: Status Quo and Future Perspectives. *Stroke* **2016**, *47*, 561−569.
(2) Morrison, H. W.; Filosa, J. A. A Quantitative Spatiotemporal Analysis of Microglia Morphology during Ischemic Stroke and Reperfusion. *J. Neuroinflammation* **2013**, *10*, 4.
(3) Wang, X.; Saegusa, H.; Huntula, S.; Tanabe, T. Blockade of Microglial Cav1.2 Ca Channel Exacerbates the Symptoms in a Parkinson's Disease Model. *Sci. Rep.* **2019**, *9*, 9138.
(4) Giaume, C.; Kirchhoff, F.; Matute, C.; Reichenbach, A.; Verkhratsky, A. Glia: The Fulcrum of Brain Diseases. *Cell Death Differ.* **2007**, *14*, 1324−1335.
(5) Dong, R.; Huang, R.; Wang, J.; Liu, H.; Xu, Z. Effects of Microglial Activation and Polarization on Brain Injury After Stroke. *Front. Neurol.* **2021**, *12*, No. 620948.
(6) Brown, G. C. Neuronal Loss after Stroke Due to Microglial Phagocytosis of Stressed Neurons. *Int. J. Mol. Sci.* **2021**, *22*, 13442.
(7) Yang, Z.; Zhao, T.-Z.; Zou, Y.-J.; Zhang, J. H.; Feng, H. Hypoxia Induces Autophagic Cell Death through Hypoxia-Inducible Factor 1α in Microglia. *PLoS One* **2014**, *9*, No. e96509.
(8) Wang, X.; Ma, J.; Fu, Q.; Zhu, L.; Zhang, Z.; Zhang, F.; Lu, N.; Chen, A. Role of Hypoxia-inducible factor-1α in Autophagic Cell Death in Microglial Cells Induced by Hypoxia. *Mol. Med. Rep.* **2017**, *15*, 2097−2105.
(9) Merlo, S.; Luaces, J. P.; Spampinato, S. F.; Toro-Urrego, N.; Caruso, G. I.; D'Amico, F.; Capani, F.; Sortino, M. A. SIRT1 Mediates Melatonin's Effects on Microglial Activation in Hypoxia: In Vitro and In Vivo Evidence. *Biomolecules* **2020**, 364.
(10) Li, K.; Wang, X.; Jiang, Y.; Zhang, X.; Liu, Z.; Yin, T.; Yang, Z. Early Intervention Attenuates Synaptic Plasticity Impairment and Neuroinflammation in 5xFAD Mice. *J. Psychiatr. Res.* **2021**, *136*, 204−216.
(11) Zhang, S. Microglial Activation after Ischaemic Stroke. *Stroke Vasc. Neurol.* **2019**, *4*, 71−74.
(12) Shahulhameed, S.; Swain, S.; Jana, S.; Chhablani, J.; Ali, M. J.; Pappuru, R. R.; Tyagi, M.; Vishwakarma, S.; Sailaja, N.; Chakrabarti, S.; Giri, L.; Kaur, I. A Robust Model System for Retinal Hypoxia: Live Imaging of Calcium Dynamics and Gene Expression Studies in Primary Human Mixed Retinal Culture. *Front. Neurosci.* **2019**, *13*, 1445.
(13) Kang, Y. B. A.; Eo, J.; Bulutoglu, B.; Yarmush, M. L.; Usta, O. B. Progressive Hypoxia-on-a-Chip: An in Vitro Oxygen Gradient Model for Capturing the Effects of Hypoxia on Primary Hepatocytes in Health and Disease. *Biotechnol. Bioeng.* **2020**, *117*, 763−775.
(14) Lewis, D. M.; Blatchley, M. R.; Park, K. M.; Gerecht, S. O2-Controllable Hydrogels for Studying Cellular Responses to Hypoxic Gradients in Three Dimensions in Vitro and in Vivo. *Nat. Protoc.* **2017**, 1620−1638.
(15) Han, M.; Zhang, Z.; Liu, Z.; Liu, Y.; Zhao, H.; Wang, B.; Zhang, C.; Shang, H.; Li, Y.; Wang, S.; Xin, T. Three-Dimensional-Cultured MSC-Derived Exosome with Hydrogel for Cerebral Ischemia Repair. *Biomater. Adv.* **2023**, *149*, No. 213396.
(16) Tang, J.; Li, Y.; Liu, X.; Yu, G.; Zheng, F.; Guo, Z.; Zhang, Y.; Shao, W.; Wu, S.; Li, H. Cobalt Induces Neurodegenerative Damages through Impairing Autophagic Flux by Activating Hypoxia-Inducible Factor-1α Triggered ROS Overproduction. *Sci. Total Environ.* **2022**, *857*, No. 159432.
(17) Zhang, H.-X.; Yang, J.-J.; Zhang, S.-A.; Zhang, S.-M.; Wang, J.-X.; Xu, Z.-Y.; Lin, R.-Y. HIF-1α Promotes Inflammatory Response of Chronic Obstructive Pulmonary Disease by Activating EGFR/PI3K/AKT Pathway. *Eur. Rev. Med. Pharmacol. Sci.* **2018**, *22*, 6077−6084.
(18) Li, Q.; Ma, R.; Zhang, M. CoCl Increases the Expression of Hypoxic Markers HIF-1α, VEGF and CXCR4 in Breast Cancer MCF-7 Cells. *Oncol. Lett.* **2018**, *15*, 1119−1124.
(19) Manohar, K.; Gupta, R. K.; Gupta, P.; Saha, D.; Gare, S.; Sarkar, R.; Misra, A.; Giri, L. FDA Approved L-Type Channel Blocker Nifedipine Reduces Cell Death in Hypoxic A549 Cells through Modulation of Mitochondrial Calcium and Superoxide Generation. *Free Radical Biol. Med.* **2021**, *177*, 189−200.
(20) Voelz, C.; Habib, P.; Köberlein, S.; Beyer, C.; Slowik, A. Alteration of miRNA Biogenesis Regulating Proteins in the Human Microglial Cell Line HMC-3 after Ischemic Stress. *Mol. Neurobiol.* **2021**, *58*, 1535−1549.
(21) Agrawal, M.; Kumar, V.; Singh, A. K.; Kashyap, M. P.; Khanna, V. K.; Siddiqui, M. A.; Pant, A. B. Trans-Resveratrol Protects Ischemic PC12 Cells by Inhibiting the Hypoxia Associated Transcription Factors and Increasing the Levels of Antioxidant Defense Enzymes. *ACS Chem. Neurosci.* **2013**, *4*, 285−294.
(22) Yin, B.; Barrionuevo, G.; Weber, S. G. Optimized Real-Time Monitoring of Glutathione Redox Status in Single Pyramidal Neurons in Organotypic Hippocampal Slices during Oxygen-Glucose Deprivation and Reperfusion. *ACS Chem. Neurosci.* **2015**, *6*, 1838−1848.
(23) Liu, Y.; Kintner, D. B.; Chanana, V.; Algharabli, J.; Chen, X.; Gao, Y.; Chen, J.; Ferrazzano, P.; Olson, J. K.; Sun, D. Activation of Microglia Depends on Na+/H+ Exchange-Mediated H+ Homeostasis. *J. Neurosci.* **2010**, *30*, 15210−15220.
(24) Zhang, B.; Yang, N.; Mo, Z.-M.; Lin, S.-P.; Zhang, F. IL-17A Enhances Microglial Response to OGD by Regulating p53 and PI3K/Akt Pathways with Involvement of ROS/HMGB1. *Front. Mol. Neurosci.* **2017**, *10*, 271.
(25) Butturini, E.; Boriero, D.; Carcereri de Prati, A.; Mariotto, S. STAT1 Drives M1 Microglia Activation and Neuroinflammation under Hypoxia. *Arch. Biochem. Biophys.* **2019**, *669*, 22−30.
(26) Zhou, H.; Zhou, J.; Teng, H.; Yang, H.; Qiu, J.; Li, X. MiR-145 Enriched Exosomes Derived from Bone Marrow-Derived Mesenchymal Stem Cells Protects against Cerebral Ischemia-Reperfusion Injury through Downregulation of FOXO1. *Biochem. Biophys. Res. Commun.* **2022**, *632*, 92−99.
(27) Lin, K.; Zhou, M.; Leng, C.; Tao, X.; Zhou, R.; Li, Y.; Sun, B.; Shu, X.; Liu, W. Neuroprotective Effect of Polyphenol Extracts from Retz. against Cerebral Ischemia-Reperfusion Injury. *Molecules* **2022**, *27*, 6449.
(28) Pavlacky, J.; Polak, J. Technical Feasibility and Physiological Relevance of Hypoxic Cell Culture Models. *Front. Endocrinol.* **2020**, *11*, 57.
(29) Gao, L.; Lin, X.; Zheng, A.; Shuang, E.; Wang, J.; Chen, X. Real-Time Monitoring of Intracellular pH in Live Cells with Fluorescent Ionic Liquid. *Anal. Chim. Acta* **2020**, *1111*, 132−138.
(30) Kioka, H.; Kato, H.; Fujita, T.; Asano, Y.; Shintani, Y.; Yamazaki, S.; Tsukamoto, O.; Imamura, H.; Kogo, M.; Kitakaze, M.; Sakata, Y.; Takashima, S. In Vivo Real-Time ATP Imaging in Zebrafish Hearts Reveals G0s2 Induces Ischemic Tolerance. *FASEB J.* **2020**, *34*, 2041−2054.
(31) Kioka, H.; Kato, H.; Fujikawa, M.; Tsukamoto, O.; Suzuki, T.; Imamura, H.; Nakano, A.; Higo, S.; Yamazaki, S.; Matsuzaki, T.; Takafuji, K.; Asanuma, H.; Asakura, M.; Minamino, T.; Shintani, Y.; Yoshida, M.; Noji, H.; Kitakaze, M.; Komuro, I.; Asano, Y.; Takashima, S. Evaluation of Intramitochondrial ATP Levels Identifies G0/G1 Switch Gene 2 as a Positive Regulator of Oxidative Phosphorylation. *Proc. Natl. Acad. Sci. U. S. A.* **2014**, *111*, 273−278.
(32) Haga, S.; Remington, S. J.; Morita, N.; Terui, K.; Ozaki, M. Hepatic Ischemia Induced Immediate Oxidative Stress after Reperfusion and Determined the Severity of the Reperfusion-Induced Damage. *Antioxid. Redox Signaling* **2009**, *11*, 2563−2572.
(33) Umpierre, A. D.; Bystrom, L. L.; Ying, Y.; Liu, Y. U.; Worrell, G.; Wu, L.-J. Microglial Calcium Signaling Is Attuned to Neuronal Activity in Awake Mice. *eLife* **2020**, *9*, No. e56502.
(34) Liu, L.; Kearns, K. N.; Eli, I.; Sharifi, K. A.; Soldozy, S.; Carlson, E. W.; Scott, K. W.; Sluzewski, M. F.; Acton, S. T.; Stauderman, K. A.; Kalani, M. Y. S.; Park, M.; Tvrdik, P. Microglial Calcium Waves

During the Hyperacute Phase of Ischemic Stroke. *Stroke* **2021**, *52*, 274−283.
(35) Sharma, P.; Ping, L. Calcium Ion Influx in Microglial Cells: Physiological and Therapeutic Significance. *J. Neurosci. Res.* **2014**, *92*, 409−423.
(36) Huang, B.-R.; Chang, P.-C.; Yeh, W.-L.; Lee, C.-H.; Tsai, C.-F.; Lin, C.; Lin, H.-Y.; Liu, Y.-S.; Wu, C. Y.-J.; Ko, P.-Y.; Huang, S.-S.; Hsu, H.-C.; Lu, D.-Y. Anti-Neuroinflammatory Effects of the Calcium Channel Blocker Nicardipine on Microglial Cells: Implications for Neuroprotection. *PLoS One* **2014**, *9*, No. e91167.
(37) McKeown, S. R.; Normoxia, D. Physoxia and Hypoxia in Tumours—implications for Treatment Response. *Br. J. Radiol.* **2014**, *87*, No. 20130676.
(38) Manole, M. D.; Kochanek, P. M.; Bayır, H.; Alexander, H.; Dezfulian, C.; Fink, E. L.; Bell, M. J.; Clark, R. S. B. Brain Tissue Oxygen Monitoring Identifies Cortical Hypoxia and Thalamic Hyperoxia after Experimental Cardiac Arrest in Rats. *Pediatr. Res.* **2014**, *75*, 295−301.
(39) Piccirillo, S.; Castaldo, P.; Macrì, M. L.; Amoroso, S.; Magi, S. Glutamate as a Potential "survival Factor" in an in Vitro Model of Neuronal Hypoxia/reoxygenation Injury: Leading Role of the Na /Ca2 Exchanger. *Cell Death Dis.* **2018**, *9*, 731.
(40) Byrne, M. B.; Leslie, M. T.; Patel, H. S.; Gaskins, H. R.; Kenis, P. J. A. Design Considerations for Open-Well Microfluidic Platforms for Hypoxic Cell Studies. *Biomicrofluidics* **2017**, *11*, No. 054116.
(41) Dhyani, V.; Swain, S.; Gupta, R. K.; Saxena, A.; Singh, R.; Giri, L. Role of Metabotropic Glutamate Receptors (mGluRs) in the Regulation of Cellular Calcium Signaling: Theory, Protocols, and Data Analysis. *Neuromethods* **2021**, 81−115.
(42) Dhyani, V.; Jana, S.; Giri, L. Gaussian Mixture Modeling of Single-Neuron Responses Obtained from Confocal-Calcium-Imaging of Dissociated Rat Hippocampal Neurons. In *2021 10th International IEEE/EMBS Conference on Neural Engineering (NER)*; IEEE, 2021.
(43) Murphy, M. P. Mitochondria and Reactive Oxygen Species. *Free Radical Biol. Med.* **2009**, *47*, 333−343.
(44) Saha, D.; Vishwakarma, S.; Gupta, R. K.; Pant, A.; Dhyani, V.; Sharma, S.; Majumdar, S.; Kaur, I.; Giri, L. Non-Prophylactic Resveratrol-Mediated Protection of Neurite Integrity under Chronic Hypoxia Is Associated with Reduction of Cav1.2 Channel Expression and Calcium Overloading. *Neurochem. Int.* **2023**, *164*, No. 105466.
(45) Weng, X.; Zhang, X.; Lu, X.; Wu, J.; Li, S. Reduced Mitochondrial Response Sensitivity Is Involved in the Anti-apoptotic Effect of Dexmedetomidine Pretreatment in Cardiomyocytes. *Int. J. Mol. Med.* **2018**, *41*, 2328−2338.
(46) Feno, S.; Butera, G.; Vecellio Reane, D.; Rizzuto, R.; Raffaello, A. Crosstalk between Calcium and ROS in Pathophysiological Conditions. *Oxid. Med. Cell. Longevity* **2019**, *2019*, No. 9324018.
(47) Snider, B. J.; Gottron, F. J.; Choi, D. W. Apoptosis and Necrosis in Cerebrovascular Disease. *Ann. N. Y. Acad. Sci.* **1999**, 893.
(48) Deb, P.; Sharma, S.; Hassan, K. M. Pathophysiologic Mechanisms of Acute Ischemic Stroke: An Overview with Emphasis on Therapeutic Significance beyond Thrombolysis. *Pathophysiology* **2010**, *17*, 197−218.
(49) Recommendations | Stroke and Transient Ischaemic Attack in over 16s: Diagnosis and Initial Management | Guidance | NICE.
(50) Khan, K. M.; Patel, J. B.; Schaefer, T. J. Nifedipine. In *StatPearls*; StatPearls Publishing: Treasure Island (FL), 2022.
(51) Razlivanov, I.; Liew, T.; Moore, E. W.; Al-Kathiri, A.; Bartram, T.; Kuvshinov, D.; Nikolaev, A. Long-Term Imaging of Calcium Dynamics Using Genetically Encoded Calcium Indicators and Automatic Tracking of Cultured Cells. *BioTechniques* **2018**, *65*, 37−39.
(52) Audero, M. M.; Prevarskaya, N.; Fiorio Pla, A. Ca Signalling and Hypoxia/Acidic Tumour Microenvironment Interplay in Tumour Progression. *Int. J. Mol. Sci.* **2022**, *23*, 7377.
(53) Kamel, H.; Iadecola, C. Brain-Immune Interactions and Ischemic Stroke: Clinical Implications. *Arch. Neurol.* **2012**, *69*, 576−581.
(54) Nandagopal, K.; Dawson, T. M.; Dawson, V. L. Critical Role for Nitric Oxide Signaling in Cardiac and Neuronal Ischemic Preconditioning and Tolerance. *J. Pharmacol. Exp. Ther.* **2001**, *297*, 474−478.
(55) Venkateswarlu, K.; Suman, G.; Dhyani, V.; Swain, S.; Giri, L.; Samavedi, S. Three-Dimensional Imaging and Quantification of Real-Time Cytosolic Calcium Oscillations in Microglial Cells Cultured on Electrospun Matrices Using Laser Scanning Confocal Microscopy. *Biotechnol. Bioeng.* **2020**, *117*, 3108−3123.
(56) Akao, M.; O'Rourke, B.; Teshima, Y.; Seharaseyon, J.; Marbán, E. Mechanistically Distinct Steps in the Mitochondrial Death Pathway Triggered by Oxidative Stress in Cardiac Myocytes. *Circ. Res.* **2003**, *92*, 186−194.

https://doi.org/10.1021/acschemneuro.2c00807
ACS Chem. Neurosci. 2023, 14, 1810−1825